Journal of Controlled Release 367 (2024) 385–401

Contents lists available at ScienceDirect

Journal of Controlled Release

journal homepage: www.elsevier.com/locate/jconrel

Quality assessment of LNP-RNA therapeutics with orthogonal analytical techniques

Jeremie Parot [a], Dora Mehn [b], Hanna Jankevics [c], Natalia Markova [c], Michele Carboni [c], Camilla Olaisen [a], Andrea D. Hoel [a], Margrét S. Sigfúsdóttir [a], Florian Meier [d], Roland Drexel [d], Gabriele Vella [e], Birgitte McDonagh [a], Terkel Hansen [a], Huong Bui [a], Geir Klinkenberg [a], Torkild Visnes [a], Sabrina Gioria [b], Patricia Urban-Lopez [b], Adriele Prina-Mello [e], Sven Even Borgos [a,*], Fanny Caputo [a,f,*], Luigi Calzolai [b,*]

[a] Department of Biotechnology and Nanomedicine, SINTEF Industry, Trondheim, Norway
[b] European Commission, Joint Research Centre (JRC), Ispra, Italy
[c] Malvern Panalytical Ltd., Worcestershire, UK
[d] Postnova Analytics GmbH, Landsberg, Germany
[e] Laboratory for Biological Characterisation of Advanced Materials (LBCAM), Trinity College Dublin, Ireland
[f] LNE - Centre for Scientific and Industrial Metrology, Trappes, France

ARTICLE INFO

Keywords:
Lipid based nanoparticles
mRNA-LNPs
Vaccines
Covid-19
Quality control
Physico-chemical properties
Particle structure

ABSTRACT

The availability of analytical methods for the characterization of lipid nanoparticles (LNPs) for *in-vivo* intracellular delivery of nucleic acids is critical for the fast development of innovative RNA therapies. In this study, analytical protocols to measure (i) chemical composition, (ii) drug loading, (iii) particle size, concentration, and stability as well as (iv) structure and morphology were evaluated and compared based on a comprehensive characterization strategy linking key physical and chemical properties to *in-vitro* efficacy and toxicity. Furthermore, the measurement protocols were assessed either by testing the reproducibility and robustness of the same technique in different laboratories, or by a correlative approach, comparing measurement results of the same attribute with orthogonal techniques. The characterization strategy and the analytical measurements described here will have an important role during formulation development and in determining robust quality attributes ultimately supporting the quality assessment of these innovative RNA therapeutics.

Abbreviations: AF4, asymmetrical-flow field-flow fractionation; API, active pharmacological ingredient; ASTM, American Society for Testing and Materials; AUC, Analytical ultracentrifugation; Cryo-TEM, cryo-Transmission Electron Microscopy; DLS, Dynamic light scattering; dRI, Differential Refractometer Index; DSC, Differential Scanning Calorimetry; DSPC, Distearoylphosphatidylcholine; EMA, European Medical Agency; EtOH, ethanol; EUNCL, European Nanomedicine Characterization Laboratory; FDA, Food and Drug Administration; FWHM, full width half maximum; HPLC, High Performance Liquid Chromatography; IRF, interferon regulatory factor; ISO, International Organization for Standardization; JRC, Joint Research Center; LC-MS/MS, Liquid Chromatography Tandem Mass Spectrometry; LDH, Lactate dehydrogenase; LDL, low-density lipoprotein; LNP, Lipid nanoparticle; MADLS, Multi-angle DLS; MALS, multi-angle light scattering; MC3, DLin-MC3-DMA (MC3, CAS Number 1224606–06-7); MD-AF4, Multidetector-asymmetric field flow fractionation; mRNA, messenger RNA; MS, Mass Spectrometry; MTT, 3-(4,5-dimethylthiazol-2-yl)-2,5-diphenyl tetrazolium bromide; NCI-NCL, Nanotechnology Characterization Laboratory; NF-κB, nuclear factor-κBeta; NMR, Nuclear magnetic resonance; NTA, Nanoparticle tracking analysis; PBS, phosphate buffered saline; PdI, Polydispersity Index; PEG-DMG, 1,2-dimyristoyl-rac-glycero-3-methoxypolyethylene glycol-2000; PSD, Particle size distribution; QA, Quality Assurance; QC, Quality control; RNA, Ribonucleic acid; SANS, Small Angle Neutron Scattering; SAXS, Small-angle X-ray scattering; SEC, size exclusion chromatography; siRNA, small interfering RNA; SM-102, Lipid H (CAS Number 2089251–47-6); SOP, standard operating procedure.

* Corresponding authors at:
E-mail addresses: SvenEven.Borgos@sintef.no (S.E. Borgos), fanny.caputo@gmail.com, fanny.caputo@cea.fr (F. Caputo), Luigi.CALZOLAI@ec.europa.eu (L. Calzolai).

https://doi.org/10.1016/j.jconrel.2024.01.037
Received 21 April 2023; Received in revised form 15 January 2024; Accepted 17 January 2024
Available online 1 February 2024

1. Introduction

Ribonucleic acid (RNA) based therapeutics are emerging as a new class of medicines that are revolutionizing the medical field. They have recently been successfully translated into clinically-approved therapies and are considered as one of the most promising technologies for the prevention and treatment of multiple diseases [1–3]. The first success story was the approval in 2018 of a small interfering RNA (siRNA) (Onpattro®) for polyneuropathy treatment in patients with hereditary transthyretin-mediated amyloidosis by the Food and Drug Administration (FDA), followed by several antisense oligonucleotide therapies *e.g.* for Duchenne muscular dystrophy [4]. The most recent examples are the messenger RNA (mRNA) vaccines (BioNTech/Pfizer, Moderna) developed at unprecedented speed against COVID-19.

The clinical translation of RNA therapies is largely dependent on the use of lipid nanoparticles (LNPs) to protect the RNA (the active pharmacological ingredient, API) from premature degradation and, at the same time, to enable uptake by host cells to deliver the RNA inside the cytosol, while being low-toxic and low-immunogenic. The recent fast regulatory approval of LNP-mRNA vaccines optimized against the SARS-CoV-2 omicron variant [5,6] highlights one of the advantages of the LNPs as delivery platforms: the capacity to easily change the mRNA payload with minimal adjustment from the initial LNP formulation.

LNPs used up to now for clinical administration have a size of around 60–150 nm and are composed of (i) ionisable lipids that complex the (ii) RNA and facilitate its escape from the cellular endosomes into the cytoplasm, (iii) polyethylene glycol (PEG)-conjugate lipids which provide stability and reduced clearance and (iv) structural lipids such as cholesterol and phospholipids. Upon the formation of the LNP-RNA, the nanoparticles are mainly held together by electrostatic and hydrophobic interactions.

It is notable that the RNA acts both as a structural component of the LNPs as well as the API. This has been recently highlighted by Hemmrich and McNeil [7] that pointed to discrepancies in the classification of lipid components as active ingredient or excipients/inactive ingredients in the regulatory assessment of the mRNA vaccines for COVID-19.

The accurate physical, chemical, and structural characterization of LNP-RNA is a prerequisite for the preclinical assessment of the quality, efficacy and safety of these complex therapeutics. This is also essential for accelerated clinical translation and cost reduction during the development process. Recently a characterization strategy for nanovaccines presented an iterative process linking both the measurement of key physical, chemical and stability properties to *in-vitro* efficacy and *in-vitro* toxicity [8].

The measurement of the key properties of complex LNP-mRNA formulations is challenging. FDA and ICH Q2R2 guidance documents applicable to the two complex LNP-mRNA COVID-19 formulations stress the need for an adequate characterization and suggest the combination of orthogonal techniques, that ideally applies a different measurement principle, for the validation of the measurement of complex quality attributes [9,10].

In this work, building from the Nanotechnology Characterization Laboratory (NCI-NCL), the European Nanomedicine Characterisation Laboratory (EUNCL) experiences [11–13] and from the characterisation assay cascade specifically focused on nanovaccines recently published by the Joint Research Centre of the European Commission (JRC) [8], we tested the proposed characterisation strategy and assessed the applicability of eight analytical techniques for measuring key properties for the pre-clinical characterization of two formulations of LNP-mRNA.

The key physico-chemical properties (size, particle concentration, density and chemical composition) were assessed with orthogonal measurements, and then associated with established *in-vitro* efficacy and *in-vitro* toxicity tests. As changes in physico-chemical properties are linked to changes in *in-vitro* efficacy and *in-vitro* toxicity, in this work we present the analytical potential of suitably selected characterisation-techniques to identify, observe and measure significant differences between i) formulations and ii) batch-to-batch variability of the same LNP-RNA system, showing the importance of the chemical composition, drug loading, particle density and structural properties over information about particle size and concentration.

Additional quality attributes of the complete formulation (the drug product, in regulatory terminology) are more mRNA-specific (such as identity and purity) [14] have not been addressed in this work.

Five expert characterisation laboratories were involved in this exercise, a minimum of three independent measurements of the same sample were performed, as summarized in Table 1. In the case of dynamic light scattering (DLS), nanoparticle tracking analysis (NTA), multidetector-asymmetric field flow fractionation (MD-AF4), and for the viability and cytotoxicity assessment measurements to assess the reproducibility of the method were performed by 2 or 3 laboratories. For the other techniques, where only one laboratory was able to perform the measurements, whenever possible, available SOPs from the EUNCL and or NCI-NCL laboratories ([15], items EUNCL-PCC-01; EUNCL-PCC-023; EUNCL-PCC-22; EUNCL-ITA-10; EUNCL-GAT-02) or standard protocols such as ISO and ASTM standards [16–19] were applied to guarantee the maximum measurement quality.

The analytical approach presented here, based on a comprehensive characterization strategy combining both physical-chemical measurements and *in-vitro* efficacy and safety assessment, is essential during both formulation development phase and product quality control and assurance, in terms of quality attribute measurement robustness. It should be noted that the quality attributes described here are non-exhaustive and, in this study, only the drug product (*i.e.*, the complete LNP-RNA formulation) has been addressed. In this respect important work is currently underway in the working party on the quality of mRNA vaccines by the Pharmacopeia European Commission [20]. This will ultimately support faster translation to clinical trials of any innovative RNA therapeutics.

2. Results & discussion

2.1. LNP-RNA synthesis

For this study two different LNP-mRNA formulations (carrying the same CleanCap® FLuc mRNA) with a different ionizable lipid were developed: one using the MC3 lipid (from here on called LNP1, mimicking the LNP-siRNA Onpattro® formulation [4]); the other using the SM-102 lipid (from here on called LNP2, mimicking the mRNA-1273 Moderna COVID-19 vaccine). In addition to the ionisable lipid (either MC3 or SM-102) the LNP1 and LNP2 were prepared starting with a lipid mixture also containing cholesterol, DSPC and PEG-2000-DMG. LNP-mRNA were synthesized by rapid mixing (in a microfluidic cartridge) the four lipids (ionisable lipid, cholesterol, DSPC and PEG-DMG in a relative molar ratio of 50:38.5:10:1.5; pre-mixed and dissolved in ethanol - 54 mg of total lipid in 8.7 mL of EtOH) with three times the volume of an mRNA solution (2.3 mg of mRNA in 26.1 mL of RNAase-free 25 mM citrate buffer at pH 4.0). The starting formulation has a total lipid / mRNA mass ratio of 23.5:1, corresponding to a N/P ratio of 6.2. The N/P ratio describes the molar ratio of the ionizable amine nitrogen atom of the ionizable lipids (N) to the anionic phosphate groups in RNA (P, one per nucleotide). This is considered a relevant attribute of LNP composition since the electrostatic attraction between these entities contributes to the formation and maintenance of the LNP internal structure. Note that other N and P atoms (*e.g.* from phospholipids) are not included in the N/P ratio.

We report here both the total lipid / RNA mass ratio and the ionisable lipid / RNA phosphate groups' molar ratios, as we consider both very important parameters that should be reported in literature to improve repeatability and reproducibility of the LNP-RNA synthesis.

During the synthesis of the different LNP-RNA batches, despite the automated mixing process, a manufacturing inconsistency was identified, noted and labelled as "manufacturing issue or glitch". This was

Table 1
Summary of the measurements performed in the study, including the laboratoriess performing the measurements and the figures and/or tables where the results are reported.

Samples analysed	Measurand	Technique	Lab(s)	Replicate(s)	Figure/Table
LNP1, LNP2–1, LNP2–2, LNP2–3	Lipid composition	nucleotide digestion followed by LC-MS/MS	Lab 1	average over 3 replicates measuring 4 nucleosides for each measurement (G, C, A, 5moU) is reported	Table 2
LNP1, LNP2–1, LNP2–2, LNP2–3	Particle size distribution	DLS	Lab 1 (DLS) Lab 4 (MA-DLS)	DLS: average over 10 replicates per sample (MA)DLS: average over 10 replicates per sample	Fig. 1 A, Lab 1 Fig. 1 B, Lab 4
LNP1, LNP2–1	Surface charge	Zeta potential	Lab 4	average over 3 replicates per sample	Table S1
LNP1, LNP2–1, LNP2–2, LNP2–3	Particle size distribution Shape factor	MD-AF4	Lab 1 Lab 2	3 replicates per sample per lab	Fig. 2, Lab 2 Fig. S5, Lab 1 Fig. 3A, Lab2
LNP1, LNP2–1, LNP2–2, LNP2–3	Particle size distribution Particle concentration	Batch NTA	Lab 1 Lab 3 Lab 4	average over 5 replicates per sample per lab	Fig. 1 C, Lab 1 Fig. S1A, Lab 4 Fig. S1B, repeatability and reproducibility in three labs
LNP1, LNP2–1, LNP2–2, LNP2–3	Particle size distribution	MD-SEC	Lab 1	average over 3 replicates per sample	Fig. S3 and Table S2, Lab 1
LNP1, LNP2–1, LNP2–2, LNP2–3	Particle size distribution Particle concentration	AF4-NTA	Lab 1	One run per sample	Fig. S6 and Table S2, Lab 1
LNP2–1, LNP2–2,	Particle structure	DSC	Lab 4	One run per sample	Fig. 3D, Lab 4
LNP1, LNP2–1, LNP2–2, LNP2–3	Particle size distribution Particle density	AUC	Lab 5	One run per sample	Fig. 1D, Lab 5 Fig. 3B-C, Lab 5 Fig. S2, Lab 5 Fig. S7, Lab 5 Table S3
LNP1, LNP2–1, LNP2–2, LNP2–3	Cytotoxicity	LDH and MTT assays on HepG2 cell lines for 24 and 48 h	Lab 1, Lab 5	average over 3 replicates per sample	Fig. 5, Lab 1 Fig. S9, Lab 5
LNP1, LNP2–1, LNP2–2, LNP2–3	Inflammatory response	IRF signalling and NF-κB in Raw-dual cells	Lab 1	average over 3 replicates per sample	Fig. S11, Lab 1
LNP1, LNP2–1, LNP2–2, LNP2–3	Complement activation	iC3b tested with commercial Enzyme-linked Immunosorbent Assay (ELISA)	Lab 5	average over 2 replicates per sample	Fig. S12, Lab 5
LNP1, LNP2–1, LNP2–2, LNP2–3	*In-vitro* protein expression	Luciferase expression in Raw Dual cells	Lab 1	average over 3 replicates per sample	Fig. 4, Lab 1
LNP1, LNP2–1,	Endotoxin contamination	LAL assay	Lab 1	average over 3 replicates per sample	Table S5, Lab 1

Table 2
Measured lipid composition, RNA loading in Total mRNA (μg/mL) measured. Average values ± standard deviations of three technical replicates.

	MC3	SM-102	Cholesterol	DSPC	DMG-PEG2000	Total lipids concentration	Total RNA	Total lipid / RNA (*w*/w)
LNP1	608 (24)	–	194 (13)	135 (5)	58 (2)	994 (44)	41 (4)	24.2
LNP2–1	–	313 (13)	133 (9)	72 (3)	42 (1)	560 (26)	26 (3)	21.5
LNP2–2	–	490 (21)	176 (12)	117 (5)	65 (2)	847 (40)	16 (2)	52.9
LNP2–3	–	498 (22)	232 (16)	116 (5)	72 (2)	919 (45)	9 (1)	101.1

particularly evident in the manufacturing of two batches (out of three) of the LNP2 formulation (the one using the SM-102 ionisable lipid). To explore the root cause of the problem and to identify the quality attribute/s impacted, the collaborating laboratories involved in this study, agreed to blindly take an in-depth characterization of 3 batches of LNP2 formulation (reported as LNP2–1, LNP2–2 and LNP2–3) as described in Table 1 and in Table 2.

2.2. Chemical composition: lipids and RNA quantification

The lipid composition and RNA content of the formulation after synthesis can be different from the starting one (*i.e.* the stoichiometry of the starting solutions). Quantifying the different lipids with a classical HPLC-based system with a UV-VIS or PDA detector is not so simple as lipids lack specific absorbance in the UV-VIS region, thus preventing the use of UV detectors. Interestingly, for the LNP-mRNA vaccines, lipid composition can be measured by HPLC coupled to corona-charge detectors as reported by BioNTech in the EMA assessment of their product [6] or by mass spectrometry (MS). In this case, we decided to develop a method based on HPLC-MS/MS, which provides high sensitivity and accuracy. The total lipids concentration can be measured with an error of around 5% and those of the individual lipids with errors ranging between 3.5% and 7% (Table 2).

The LNP1 and LNP2 formulations had a starting total lipid concentration of 1.5 mg/mL and mRNA concentration of 68.2 μg/mL. Results reported in Table 2 show that for all samples there was a substantial loss of lipids in the manufacturing process, resulting in concentration of total lipids lower than the initially added amount of 1.5 mg/mL, yielding total lipid mass of 0.99 mg/mL for LNP1 and showing great variabilities among LNP2 batches (0.56, 0.85 and 0.92 mg/mL for LNP2–1, LNP2–2, and LNP2–3, respectively). It is interesting to note that the relative molar ratio of the four different lipids in the four samples are very similar to the expected values (50: 38.5: 10: 1.5) with the most different one being sample LNP2–3 having ratios of 47.3: 40.5: 9.9: 2.0.

The quantification of RNA is a more complex and challenging issue. The total RNA content can be measured using fluorescence methods. However, these methods show questionable accuracy when applied to measure mRNA loading [21]. To improve the analytical confidence, we developed a method based on LC-MS/MS, for direct, label-free detection of all the mRNA single nucleosides after enzymatic depolymerization and dephosphorylation (see materials section for details). Knowing the theoretical nucleotide composition, this method can quantify mRNA based on each constituent nucleoside. The developed LC-MS/MS methodology can also directly quantify modified bases as a result of either intentional incorporation (*e.g.* 5-methoxy-uridine, as it happens in the BioNTech/Pfizer and Moderna COVID-19 vaccines) or base damage (*e.g.* 7,8-dihydro-8-oxoguanine). The results in Table 2 show that total encapsulated mRNA can be quantified with a reproducibility error of

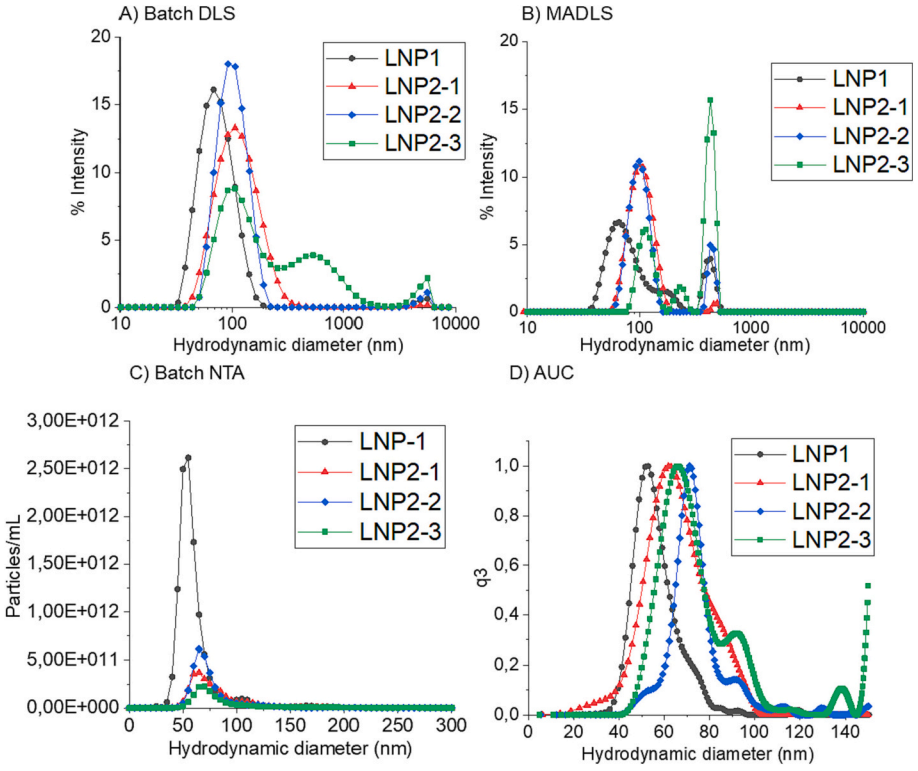

Fig. 1. Hydrodynamic diameter measured by batch DLS, MADLS, NTA and AUC of LNP1 (black curve), LNP2–1 (red curve), LNP2–2 (blue curve) and LNP2–3 (green curve). The average particle size distribution (PSD) calculated over 3 (NTA, MADLS) or 10 (DLS, MADLS) measurements is reported. For AUC a representative PSD measured in PBS at 60% D_2O is shown (single measurement). (For interpretation of the references to colour in this figure legend, the reader is referred to the web version of this article.)

Table 3
Comparison of the particle size and polydispersity measurements performed by batch DLS, MADLS, MD-AF4, SEC-MALS, Batch NTA, AF4-NTA and AUC. When replicate measurements are performed the mean values (SD) measured by each laboratory are reported.

Sample	Batch DLS		MADLS			MD-AF4			SEC-MALS	Batch NTA (Lab 4)		AF4-NTA*		AUC	
	z-ave (nm)	PdI	D50 (nm)	Span	Particles/mL	Dg (Berry) nm	z-ave nm	Shape factor	Dg (Berry) nm	D50 nm	Particles/mL	D50 (mode) nm	Particles/mL	DStokes* (mode) nm	Particle density (g/mL)
LNP1	70.1 (0.5)	0.15 (0.01)	55 (3)	0.92 (0.17)	6.7.E+12 (2.7 E+12)	47 (1)	74 (3)	0.64 (0.04)	54 (2)	53.2 (0.78)	1.2 E+13 (4 E+12)	57	1.7 E+12.0	53	0.962 (0.008)
LNP2–1	103 (1)	0.16 (0.02)	91 (4)	0.66 (0.08)	5.1 E+11 (1.5 E+11)	77 (4)	92 (3)	0.83 (0.06)	68 (1)	69.8 (0.86)	2.6 E+12 (5 E+011)	65	9.7 E+11.0	62	0.973 (0.006)
LNP2–2	102 (1)	0.21 (0.01)	83 (8)	1.53 (1.26)	8.0 E+10 (5.9 E+10)	65 (1)	89 (4)	0.73 (0.04)	64 (1)	67.1 (0.64)	3.1 E+12 (1 E+11)	70	2.8 E+12.0	71	0.945 (0.008)
LNP2–3	167 (4)	0.51 (0.05)	153 (12)	4.49 (3.37)	1.1E+12 (1.5 E+12)	102 (4)	109 (5)	0.94 (0.08)	60 (1)	72.1 (0.53)	1.49 E+12 (1 E+010)	71	2.6 E+12.0	66	0.910 (0.01)

Average values (SD) are reported except for AUC where one measurement result is shown. AUC data correspond to the measurements performed in PBS containing 60% D_2O(*).

around 10% for the different samples.

The concentration of RNA in all samples is well below the expected value of 68.2 μg/mL, but LNP1 and LNP2–1 have mass ratio to total lipid very close to the expected value of 23.5 (24.2 and 21.5, respectively, see Table 2). Conversely, samples LNP2–2 and LNP2–3 contain considerably lower amounts of RNA to total lipid mass (ratio of 52.9 and 102.1, respectively) to what was expected.

Different types of material loss and dilution effects can take place in the formulation process: during microfluidic synthesis the first and last part of the reaction solvent are usually discarded to improve homogeneity, reduce particle size and polydispersity. Also, some lipids and mRNA could be lost due to incomplete inclusion in the particle formation and will thus remain as free molecules that could be dialyzed away (lipids) or degraded (mRNA). Finally, dilution effects can occur during the dialysis step. All this combined could easily explain the significant reduction of total lipid and RNA concentration compared with the expected values. On the other hand, for samples well-formed (*i.e.* LNP1 and LNP2–1) the lipids' relative molar ratios and the total lipid to RNA mass ratio are very close to the expected values.

In the case of LNP2–2 and LNP2–3, the significant reduction of RNA compared to lipid mass is a key indicator that something happened during the synthesis. The joint hypothesis of the labs involved is that LNP2–2 and LNP2–3 incurred some problems during the formulation process. Furthermore, when undertaking further manufacturing process inspection this was narrowed down to the syringe inlet connected to the microfluidic cartridge which did not correctly control the ratio between the organic phase containing the lipid components and the aqueous phase containing the mRNA. Nevertheless, these two "failed" batches provided an excellent starting point for a blinded study assessing the analytical power of the techniques applied in this work, and thus for their suitability in quality control of LNP-mRNA.

2.3. Particle size and concentration

Size is considered a critical quality attribute of LNP-mRNA vaccines: it directly influences both the biodistribution and the immunogenicity [22]. In the nanomedicine field, the consensus is that particle size distribution (PSD) should also be measured, in addition to the average size [23]. Measuring PSD and particle concentration of LNP systems can be particularly challenging. In our case, we adopted six among the most used techniques including batch sizing and hyphenated techniques combining fractionation of polydisperse samples coupled by online sizing measurements, as reported in Table 1. Results obtained are presented below.

2.3.1. Dynamic light scattering: a useful tool for preliminary assessment of particle size

DLS is a long-standing, fast and very widespread technique for sizing and quality control of nanoparticles [23]. As a first approach for sizing the four LNP-mRNA formulations, we applied batch DLS in two independent labs, in its two available configurations, single angle DLS (Fig. 1A) and multi-angle (MA)DLS (Fig. 1B). These were then complemented with two (batch) techniques used for the analysis of LNP-RNA: nanoparticle tracking analysis (NTA), measured independently in three laboratories [24] and analytical ultracentrifugation (AUC) [25]. The average particle size distribution calculated over the measured replicates by each lab (Fig. 1A-B) and the average numerical calculated size values (Table 3) measured by batch DLS or (MA)DLS independently identify two key features: i) a smaller size (hydrodynamic diameter) of LNP1 (z-ave = 70 ± 1 nm) compared to LNP2 (z-ave = 103 ± 1 nm) as main peak in all batches, and ii) a notable second population of aggregates in batch LNP2–3, with a significantly larger size (>500 nm). Size polydispersity was comparable and acceptable for LNP1, LNP2–1 and LNP2–2 (PdI = 0.15, 0.16 and 0.21, respectively by DLS), whereas it was dramatically increased for LNP2–3 (PdI = 0.51 by DLS).

2.3.2. Nanoparticle tracking analysis: an orthogonal method for particle size. Some issues with LNPs dilution

NTA measurements, which are also based on dynamic light scattering and Brownian motion yet in a single-particle tracking mode, also provide particle size. The results of the average particle size distribution measured over 5 replicates by each of the three labs involved in the study (Fig. 1C and Table 3) indicate that LNP1 formulation is slightly smaller than LNP2–1 (as shown by DLS). NTA also gives a complementary insight into the second population of large particles present in LNP2–3. In fact, NTA measures the size of each particle, while DLS tends to overestimate the number of larger particles compared to smaller ones. Both methods are based on the measurement of the Brownian motion of the particles, which limit the measurable upper size to around 1 μm, thus limiting the possibility to measure large aggregates [26]. Based on the same physical principle, NTA and DLS cannot be considered orthogonal to each other.

In addition to size, NTA can directly measure particle concentration. Results from the measurements performed in three laboratories showed an intralaboratory coefficient of variation (SD/Mean value %) of around 20% in the measurement of particle concentration and an even larger interlaboratory variation, especially with regards to concentration values of LNP2 samples (Table S1). Those data indicated the lack of repeatability and reproducibility of batch NTA to measure the particle concentration of the LNPs formulations considered in this study, despite its common use to characterise LNP-RNA in the community. To assess the possible source of this high variability, we repeated the concentration measurements within a short interval (10 min) in each lab and observed the variation within single measurement runs on the same sample over a short measurement time. As shown in Fig. S1 the concentration measured for LNP2 dropped significantly between the replicates, while LNP1 was less affected but still showing variability between replicates. To set optimal recording and measurement conditions with the NTA, the samples must be adequately diluted to have accurate readouts. We therefore concluded that particular care should be taken when using NTA to measure particle concentration and size of LNP formulations that could be unstable when highly diluted. Thus, NTA can be suitable only if the stability of the analysed formulation has been previously checked in the analytical conditions used. Satisfactory measurement conditions have not been achieved in this study, despite 3 expert labs have been involved. Our results highlight that NTA would require customised SOP to identify the optimal sample preparation, dilution and injection mode compared to relevant LNP controls to reduce, if not remove, any bias or intrinsic measurement issues. To optimize the measurement conditions we suggest to perform repeated measurements at different time points within a short measurement window to assess the measurement repeatability. In case a better repeatability is achieved than in our study (coefficient of variation for measured particle size and concentration < 5–10%, depending on the needs), it may be still useful to compare the results obtained using orthogonal or complementary methods to validate the measured results.

2.3.3. Analytical ultracentrifugation is a robust, high resolution, method to measure size and density

AUC was used as a third batch technique, orthogonal to NTA and

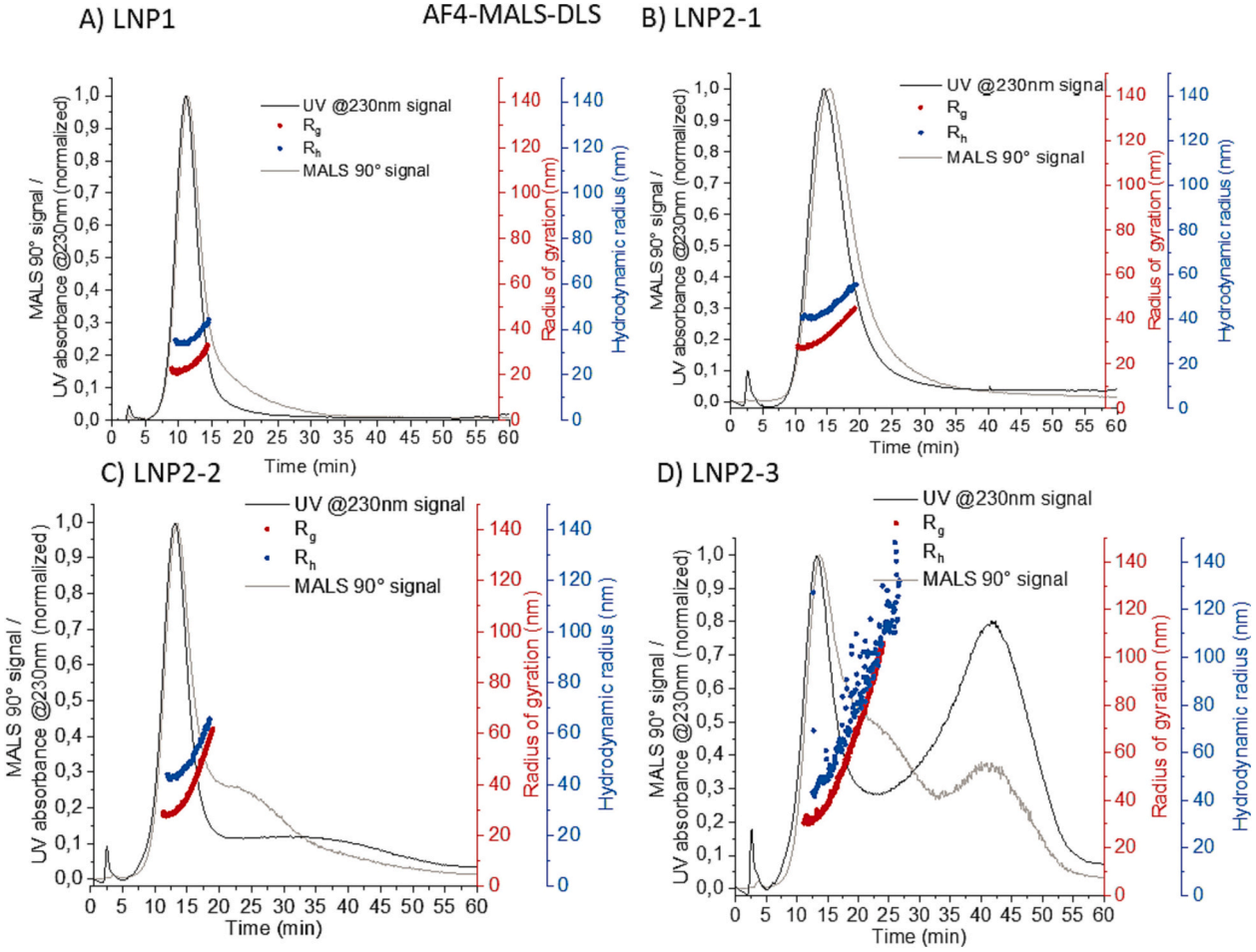

Fig. 2. Size and polydispersity by AF4-MALS-DLS. Representative fractograms (one measurement run selected within 3 replicates) of A) LNP1, B) LNP2–1, C) LNP2–2 and D) LNP2–3 reporting the UV-VIS (black curve), the MALS scattering intensity at 90° (grey curve), the hydrodynamic radius (Rh, blue curve) and the radius of gyration (Rg, red curve). (For interpretation of the references to colour in this figure legend, the reader is referred to the web version of this article.)

DLS, for measuring the particle size distribution and polydispersity of the same samples. AUC (Fig. 1D) confirmed the findings obtained by DLS; LNP2–1 showed a larger Stokes diameter than LNP1. LNP2–2 has a narrow size distribution, but also contained a population (about 12 *w*/w %) with larger particles. LNP2–3 presented a wider size distribution and most probably contained larger aggregates. Interestingly, looking at the sedimentation coefficient distribution (Fig. S2), LNP2–3 sediments significantly slower than the other samples. From these measurements and results, our findings strongly suggest that a change occurred in the intra-particular structure, towards a less condensed composition with lower density and a larger hydrodynamic diameter, as observed by batch DLS.

2.3.4. *Hyphenated techniques for the measurement of size and concentration: higher resolution but increased complexity*

Fractionation techniques, such as size exclusion chromatography (SEC) or asymmetrical-flow field-flow fractionation (AF4), allow separation of different LNP populations with increased size-resolving power and can be coupled to online particle size measurements. The fractionation process should not impact the LNP physical integrity or retain a part of the sample within the column or in the channel.

The results of the SEC fractionation coupled to multi-angle light scattering (MALS) detection are reported in Fig. S3 (3 single runs are shown to assess the repeatability of the protocol), while the diameter of gyration measured by online MALS (1st order Berry model) averaged over the full width half maximum (FWHM) are shown in Table 3 and in Table S2. The SEC fractogram, in accordance with DLS and AUC results, showed a larger size for LNP2–1 *vs* LNP1 (diameter of gyration, Dg, of 74 *vs* 90 nm). However, no difference between LNP2 batches was detected. Moreover, the mass recovery (the ratio between the mass fractionated and the mass injected) was <60%. This low mass recovery could be due to large aggregates in batches LNP2–2 and LNP2–3 not eluting from the SEC column. The inability of SEC-MALS to properly fractionate larger particles could explain why it could not detect differences between the LNP2 batches. Overall, SEC-MALS measurements were repeatable, but the results were difficult to reconcile to the ones obtained with different, orthogonal, techniques, probably due to the loss of a part of the LNP population not eluted from the SEC column.

AF4 coupled online to MALS and DLS (AF4-MALS-DLS) is one of the most powerful techniques for the accurate analysis of liposomes [11,27–29]. The AF4-MALS-DLS measurements were performed in two different labs according to the method reported in Fig. S4 [29]. The AF4-MALS-DLS fractograms of the four LNP samples are reported in Fig. 2. Acceptance criteria defined by the *ISO/TS 21362:2018 Nanotechnologies — Analysis of nano-objects using asymmetrical-flow and centrifugal field-flow fractionation* [30], such as mass recovery, repeatability and reproducibility of the fractionation process and of the sizing measurements were found to be acceptable as shown by replicate measurements in Table S2 and Fig. S5.

In line with DLS and AUC measurements, the LNP1 and LNP2–1 appear rather monodispersed, while a shoulder both in UV-VIS and MALS signals following the main peak indicates the presence of larger

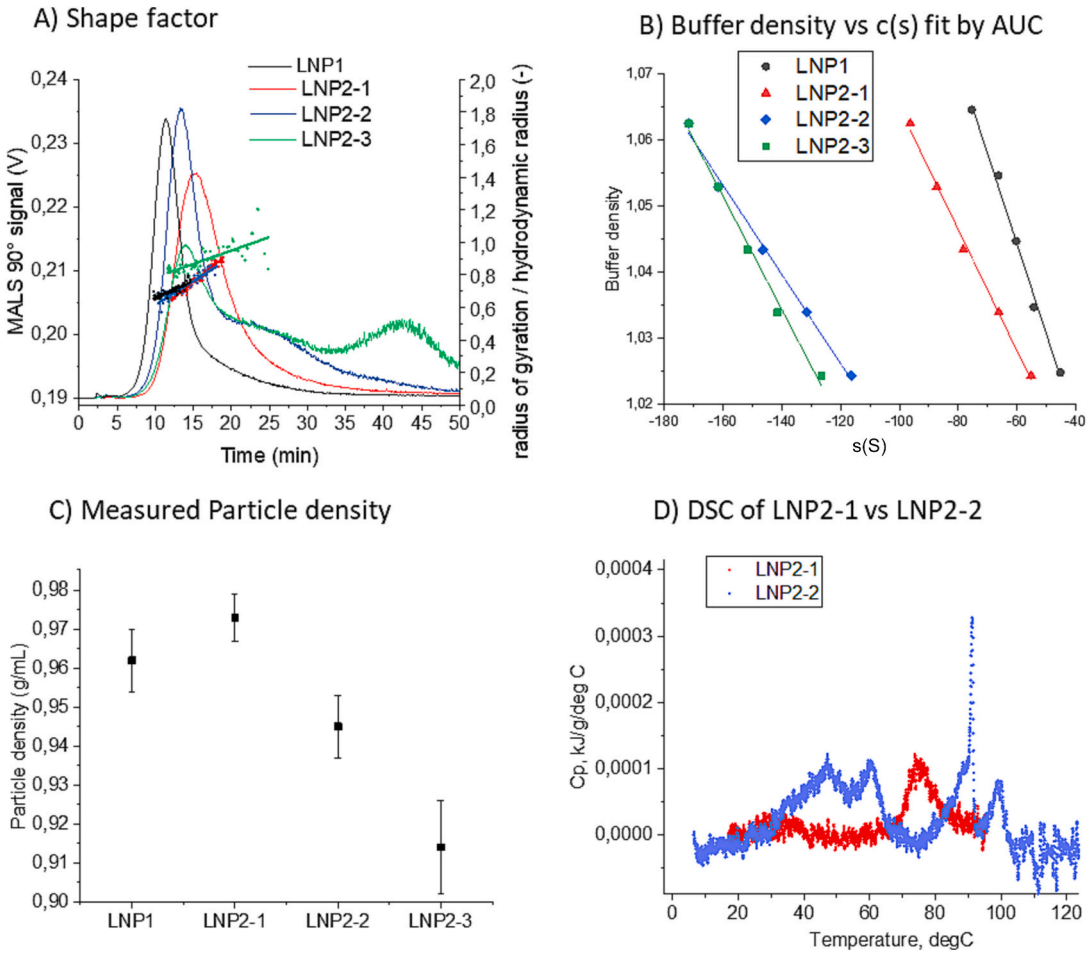

Fig. 3. Particle morphology and density by AF4-MALS. A) shape factor reported over the MALS elution profile measured by AF4-DLS-MALS for LNP1 and for the LNP2 batches, one representative fractogram is reported B) fit of the average c(s) *vs* the buffer density measured by AUC in PBS at different H_2O/D_2O%, C) measured particle density (SD = 2*SE at 95% confident interval) and D) DSC overlays of LNP2–1 and LNP2–2 normalized per mole of mRNA for each sample and expressed as apparent excess heat capacity. One representative DSC run is reported.

particles in both two LNP2 (LNP2–2 and LNP2–3).

Results confirmed that, as for other nano-pharmaceuticals and vaccines [11,23,27,29], AF4-MALS can reliably measure batch-to-batch variability, allowing to identify and understand small (but significant) differences in the particle size distribution as well as potential presence of different populations, hence being able to evaluate the physical stability of LNPs-mRNA.

AF4 can also be coupled online to NTA to measure the particle number concentration of the different size species eventually present in polydisperse samples. The coupling of the two systems was realized using a flow splitter to deliver the sample at an appropriate flow speed for the NTA measurements and by adapting the injected concentration to optimize the number of particles/frames visualized by NTA. Results obtained are reported in Table 3 and showed in Fig. S6. This "early-stage" combined analytical technique seemed to provide another way to directly measure particle number concentration, helping to solve the instability issues experienced by NTA in batch mode in the case of LNP-2.

2.3.5. Conclusions from the particle size distribution measurements

Fig. S7 reports the measured average size and particle concentration for all techniques applied in the study. To summarize, for sample LNP-1 all the measurement methods indicate an average particle size below 80 nm, as expected (DLS, NTA and AUC in batch mode, AF4 and SEC hyphenated with MALS, NTA or DLS online). Measurement values may be slightly, but significantly, different due to the intrinsic differences in the sizes detected (hydrodynamic, or geometric diameter), however, results are coherent and are corroborating each other (Table 3, first row). For the three different LNP2 batches, while batch NTA and SEC-MALS are not detecting significant differences, probably due to the instability issues (NTA) or to the inability to fractionate larger particles and/or to destabilise the LNP integrity due to the interaction between the stationary phase and the particles (SEC-MALS), DLS clearly identified batch LNP2–3 as an outlier (due to its larger size and polydispersity; Table 3). AUC, MA-DLS, and AF4-MALS identified both batches LNP2–2 and LNP2–3 as different from LNP2–1 (due to the different median size and lower density; Table 3), showing higher resolution in detecting multiple populations in polydisperse samples.

2.4. Particle density, morphology, and structure

Particle density, morphology and structure can be used to quickly assess the quality of different formulations or production batches. Morphology and particle density can be obtained as complementary information from AF4-MALS-DLS and AUC measurements, respectively.

2.4.1. Morphology by AF4-MALS-DLS

AF4-MALS-DLS can measure the shape factor, which is the ratio between Rg (radius of gyration determined by MALS) and Rh (hydrodynamic radius determined by DLS), providing indirect information about the particle shape. For spherical particles with a uniformly dense core (such as the LNPs) a shape factor ρ of 0.8–0.65 is expected because the scattering centres are distributed closer to the centre of mass and thus $Rg < Rh$. On the other hand, a value of $\rho = 1$ would be associated with hollow sphere morphology (as in the case of empty liposomes), where $Rg = Rh$. Fig. 3A shows ρ calculated *vs.* the elution time of the LNP samples. The measurements indicate that the LNP1 formulation has a more compact structure than the LNP2 formulations. Moreover, within the three LNP2 batches, LNP2–3 has a much higher Rg/Rh ratio closer to 1 (hollow particle).

2.4.2. Particle density by AUC

AUC can also measure particle density following various approaches described in ISO 18747-1 and ISO 18747-2. The latter standard foresees the measurement of migration velocity of the particles "dispersed into at least two continuous phases of different densities, driven by gravitational or centrifugal fields". We have followed this approach, applying the strategy reported by Henrickson et al. [25]: the migration velocity of the floating particles was measured separately in more than two (in our case five) aqueous buffers of variable density. Plotting the mode of the sedimentation coefficient distribution (ls-g*(s)) *vs* the density of the different buffers (Fig. 3B and Fig. S8) allows determining the intercept. The intercept represents the density of the buffer where there is no sedimentation or floatation (zero migration velocity) indicating that the densities of the buffer and of the particles are the same. This allowed us to measure the density of the LNPs under investigation (Table S3, Fig. 3C).

The density values measured with AUC fit well with the values predicted using the measured lipid and RNA composition of the different samples (Table S3). LNP2–1 has a slightly higher measured density than LNP1 reflecting the higher RNA to lipid ratio. The LNP2–2- and LNP2–3 batches show a significantly lower density in line with their lower content of mRNA measured by LC-MS/MS. Overall, results from AUC showed that it can measure both size and density of LNP-mRNA systems and can easily identify differences between various batches of the same formulation.

2.4.3. Particle structure by differential scanning calorimetry

Differential scanning calorimetry (DSC) can provide a higher-level fingerprint of the LNPs' structure and composition and flag structural and compositional differences between batches, which may be sufficient for quality control (QC) purposes. Previous results show that well formed LNP-mRNA formulations have a main peak in the thermogram with a melting temperature (Tm) of around 75 °C [24]. Fig. 3D and Table 4 reports the results for batches LNP2–1 and LNP2–2: it is immediately clear that the two samples have significantly different structures. Sample LNP2–1 has a main peak with a melting temperature of around 75 °C, while LNP2–2 shows at least two transitions at much lower temperatures (45 °C and 60 °C). Even if it is not possible to discern the nature of the different thermal transitions, from these limited set of DSC measurements, the results clearly indicate that sample LNP2–2 has a very different structure from sample LNP2–1.

In general, based on the wealth of publications on DSC in application to lipids, nucleic acids and their complexes, and considering the composition of the LNP samples in this study, the observed peaks could be reflecting transitions related to structural changes in mRNA molecules and concomitant thermotropic transitions associated with the lipids forming LNP particles.

2.5. Measuring in-vitro potency and toxicity

The *in-vitro* measurement of potency and toxicity are key steps in the pre-clinical characterization, before moving into the more complex and expensive animal studies. Potency of a given RNA formulation depends on the uptake of the LNP-mRNA by cells and the expression of the encoded protein (an antigen, in the case of LNP-mRNA vaccines). In

Table 4
Summary of the results of DSC measurements of LNP2–1 and LNP2–2 samples. NA: not available.

Sample	Tm1, ^{0}C	Tm2, ^{0}C	Tm3, ^{0}C	Tm4, ^{0}C	Tm5, ^{0}C	Total area, mJ
LNP1 [24]	20.9	71.7	NA	NA	NA	0.633
LNP2–1	25.6	75.0	NA	NA	NA	0.204
LNP2–2	24.0	47.2	60.4	91.0	99.3	0.787

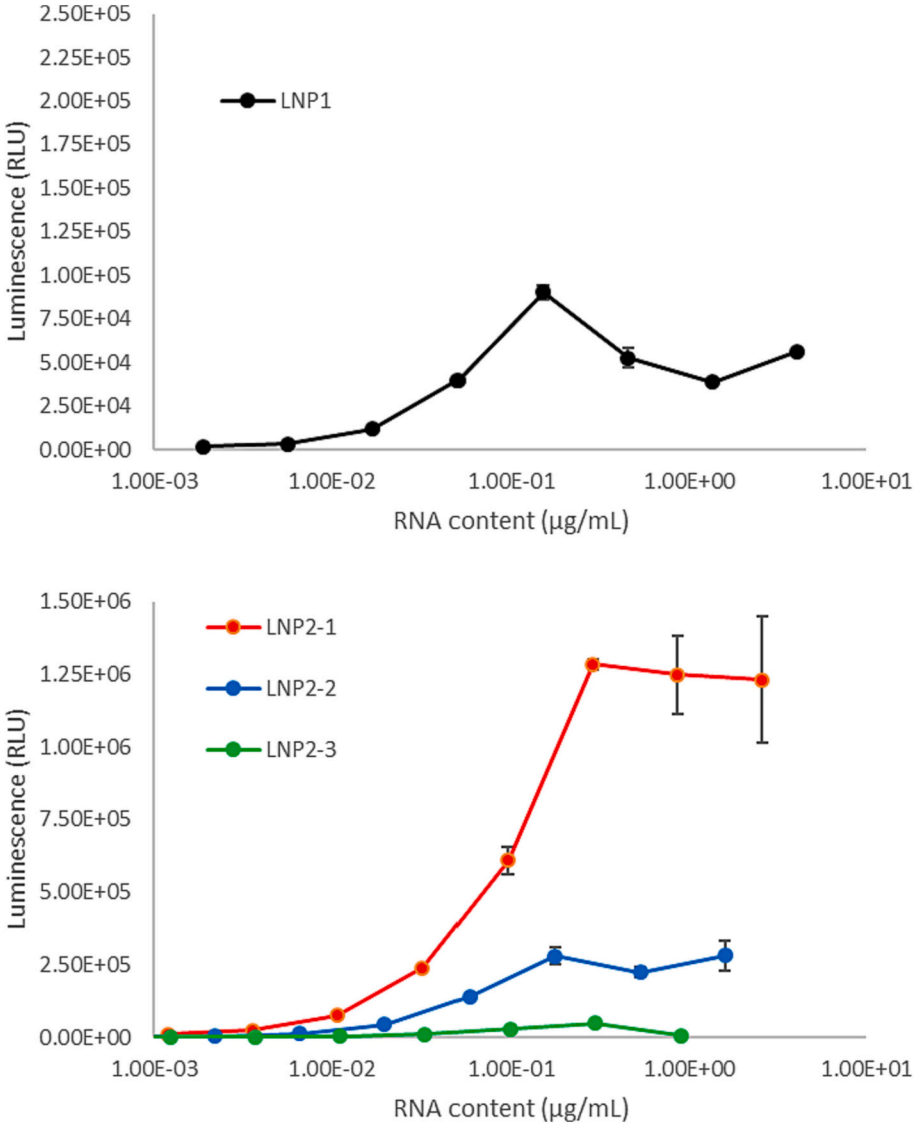

Fig. 4. Functional luciferase mRNA assays for LNP1 (upper panel and LNP2 batches (bottompanel): Luminescence readings from Hep G2 cells treated with the indicated LNP-mRNA complexes for 24 h. Data are average ± standard deviation from three technical replicates, normalized for total RNA content.

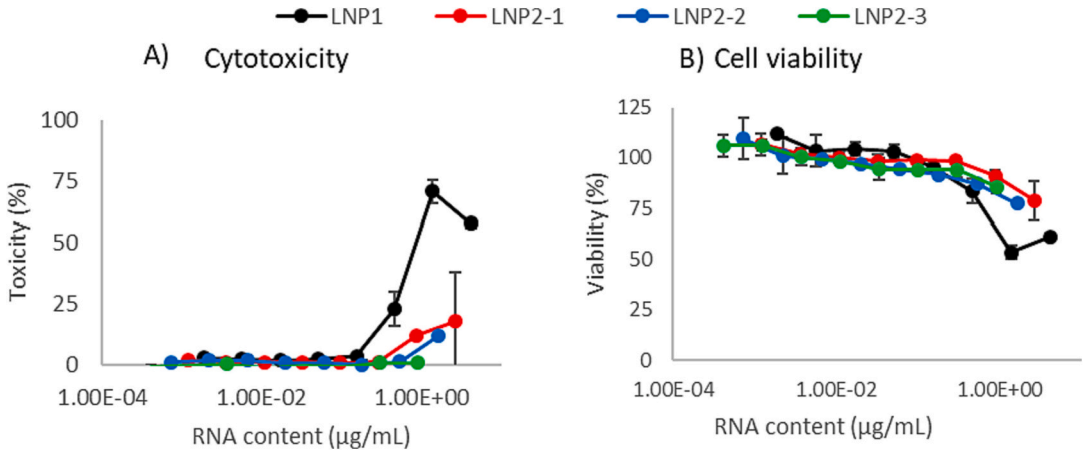

Fig. 5. Cytotoxicity assays. (A) Toxicity measured as LDH release from Hep G2 cells treated with the indicated LNP-mRNA complexes and (B) MTT viability of Hep G2 cells treated with the indicated LNP-mRNA complexes for 24 h. Data are normalized for total RNA content. Data are all average ± standard deviations of three technical replicates.

particular, potency can be evaluated *in-vitro* by cell-culture-based assays able to measure the amount of functional protein that is translated; for our study we used *in-vitro* luciferase expression. Toxicity was instead evaluated by monitoring cytotoxicity, using the MTT and LDH assays as recommended by the Standards [16,18] and by assessing inflammatory response (interferon regulatory factor -IRF- and nuclear factor-κBeta -NF-κB- inflammation assays). Presence of endotoxins could severely interfere with *in-vitro* assays. To verify endotoxin contamination of the formulations, the recombinant factor C assay was performed.

2.5.1. In-vitro luciferase expression

The LNP-mRNA formulations used in this study encode the firefly luciferase enzyme, thus allowing setting up a cell-culture-based assay using the chemiluminescence emission (catalysed by the luciferase enzyme) as read-out. Hep G2 cells were transfected with the four different LNP-mRNA samples, their non-encapsulated mRNA counterpart, or corresponding positive (cells transfected with FLuc mRNA using commercial transfection agent) and negative control (cells exposed to commercial transfection reagent alone). Luciferase activity was measured 24 h after transfection to assess cell uptake and intracellular translation from the mRNA to functional luciferase. Results indicated that, in general, LNP2 has higher luciferase activity than LNP1 formulation (Fig. 4). A quantitative comparison of the expression values measured for the two formulations needs to consider several factors including LNP composition, formulation buffer, RNA loading and particle structure. At the same time, the higher luciferase activity of LNP2 is observed even at the higher (100×) dilutions.

Importantly, a quantitative comparison of the luciferase expression can be made for the three LNP-2 batches (all prepared in sucrose), with LNP2–1 approximately 5× times higher than LNP2–2, whereas LNP2–3 luciferase expression was almost negligible.

These results agree with the physico-chemical observations that indicate that LNP2–3 had different size and density with respect to the other two formulations. The batch LNP2–2 was interesting: in fact, a slight increase in polydispersity (observed from the batch mode sizing techniques), and the different structure and density inferred from DSC and AUC, translates into a very significant (around 5-fold) reduction in *in-vitro* potency compared to LNP2–1. This confirms that the small differences between batches, observed by fractionation-based analyses (AF4-MALS-DLS) as well as by other techniques capable of discerning intra-particular structure (AUC, DSC), carry a clear functional relevance.

2.5.2. In-vitro toxicity: the effect of lipid composition

In the clinical translation of mRNA medicines, verification of their safety precedes any other biological investigation. To evaluate the toxicity of the compounds, we selected and performed a panel of relevant *in-vitro* toxicity assays, specifically lactate dehydrogenase (LDH) and 3-(4,5-dimethylthiazol-2-yl)-2,5-diphenyltetrazolium bromide (MTT) cytotoxicity assays, and assays for inflammatory responses driven by interferon regulatory factor (IRF) and nuclear factor-κBeta (NF-κB). Endotoxin contamination was also performed as a pre-screening prior to measuring the inflammatory response, showing negative results for all the batches tested as reported in Table S5. Briefly, both NF-κB and IRF-driven inflammation can be triggered by extracellular cytokines and pathogens, as well as intracellular damage- and pathogen-associated molecular patterns, such as double-stranded RNA, or the presence of unmodified uridine in mRNA. Importantly, both inflammation pathways are shown to be triggered by mRNA-LNP therapeutics [31]. The LDH assays provided a simple and reliable method for determining cellular cytotoxicity by measuring the release of the LDH cytosolic enzyme into the cell culture medium upon damage to the plasma membrane, while the MTT assay uses a synthetic dye (3-(4,5-dimethylthiazol-2-yl)-2,5-diphenyltetrazolium bromide) to determine mammalian cell viability. The redox potential in live mammalian cells reduced MTT to a strongly pigmented formazan product that can be read by an optical detector. Results obtained by two laboratories are reported in Fig. 5 and Fig. S9. Results showed that the MC3-based formulation (LNP1) induced significantly higher cytotoxicity (both in terms of damaged cell membrane and cell viability) than those based on the SM-102 lipid (LNP2). The three different LNP2 batches showed quite similar behaviour, with limited toxicity observed only at the highest doses tested. These data were in line with morphology observation and representative images of cell exposed for 24 h to the different LNPs can be found in Fig. S10.

None of the samples show any significant inflammation response (apart for LNP1 at the highest dose) (Fig. S11). In addition, there was no significant difference in complement activation (as measured by the amount of iC3b levels, Fig. S12) between the four different samples (LNP1 and the three different batches of LNP2), although iC3b production was around two-fold higher in respect to the negative control (PBS).

2.6. Linking physico-chemical properties to potency

The performances of the assays tested in this work are summarized in Table 5. The results presented, underline some specific issues that merit a detailed discussion.

Linking chemical composition and RNA loading to structural properties and efficacy of the formulation is a key aspect that should be considered not only during formulation development but also during QC. The concentration of lipids and mRNA in the final formulation could be quite different from the expected values and should be measured for each batch as part of the full manufacturing quality assurance (QA). As presented, it is evident that small variations in operating conditions of the microfluidic system may induce a very significant difference in the lipid/RNA ratio, as for the case of LNP-2 batch 2 and 3. This variation influences the complex structural properties of the LNP-RNA and can lead to significant changes in the safety- and efficacy profiles of the formulation. Differences in the intra-particle structure can be immediately highlighted by DSC, a technique widely used, and accessible for QC purposes that can be used as the first screening approach to detect structural differences by looking at the thermal transition fingerprint of the complex LNP-RNA structure. During formulation development, or when a further understanding of the particle structural properties is needed, AUC could be used to measure both particle size distribution and particle density. In addition, AF4-MALS-DLS could be used for particle morphology beyond batch DLS, before getting into more detailed structural investigations by highly complex, and not easily accessible techniques, such as small-angle X-ray scattering (SAXS), small angle neutron scattering (SANS), nuclear magnetic resonance (NMR) or cryo-transmission electron microscopy (cryo-TEM) [32–34].

The measurement of physical properties such as particle size and polydispersity may indicate some differences between batches but cannot identify the very significant differences in RNA loading, particle structure and efficacy experienced in this study among batches (example of LNP2–1 *vs* LNP2–2 or LNP2–3). DLS is confirmed to be a very fast screening technique for polydispersity and physical instability issues. If higher resolution is needed AF4-MALS-DLS is a robust hyphenated alternative to batch techniques. On the other hand, SEC is not suitable to measure aggregation and physical stability of LNP-RNA, due to the limitation in the particle recovery and maximum detectable size (at around 200 nm in diameter).

The measurement of particle concentration is still suffering from reproducibility issues. Particle instability at the dilution required to achieve optimal measurement conditions (5000–2000×) could affect the results of NTA measurements, as shown in this work by the low repeatability and reproducibility independently experienced by three labs (coefficient of variation for concentration measurements >20%). In the absence of reference materials that could be used for method validation, indirect measurements of particles concentration with orthogonal approaches could be used to unmask the experienced bias. Examples are approaches such as (MA)DLS [24] or AF4-MALS [29]. However, they both require *a priori* knowledge of the refractive index of

Table 5
Comparison of the complementary methods for the QCs considered in this paper, according to their physical principle, applicability, size range, performances in resolution for size and concentration measurements, sample needs, costs, and measurement complexity. In the case of mRNA loading, other widely used techniques not considered in this work are also considered for comparison.

Attribute(s)	Measurement technique	Measurands	Physical principle	Applicability	Possible bias	Cost, measurement complexity	Suggested for QC? (1–3)
Physical properties: Particle size distribution, Particle concentration, Polydispersity, Physical stability	Batch DLS/ MADLS	Size: Rh Polydispersity: PdI (or span) Particle concentration (for MADLS only)	Brownian motion detected by dynamic light scattering	Monodispersed samples (PdI < 0.3)	Low resolution for polydispersed samples	Cost: low Measurement complexity: low	3
	NTA	Size: Rh Polydispersity: Span Particle concentration	Brownian motion detected by light scattering	Only for stable samples	Particle instability upon dilution	Cost: low Measurement complexity: medium	1
	SEC-MALS	Rg	SEC: separation by size MALS: static light scattering	For Rg <200 nm, if mass recovery is >70%.	Large particles are retained in the column	Cost: medium Measurement complexity: medium	1
	AF4-MALS-DLS	Size: Rg (Rh) Shape factor Rg/Rh Polydispersity Particle concentration	AF4: separation by size MALS: static light scattering DLS: Brownian motion detected by dynamic light scattering	If mass recovery is >70%.	Particle instability may be induced during the focusing step prior to fractionation	Cost: medium Measurement complexity: medium	3
	AF4-NTA	Rh, particle concentration	AF4: separation by size NTA: Brownian motion detected by light scattering			Cost: medium Measurement complexity: high	2
Structure and morphology	AUC	Particle density Particle size	Particle sedimentation by stoke law	yes	Particle density must be measured/known to calculate particle size	Cost: medium Measurement complexity; high	3
	DSC	Structural information associated to thermal transitions	temperature and heat flow associated with material transitions as a function of time and temperature	yes	Useful fingerprint for QC, detailed structural info must be complemented with SAXS, SANS	Cost: medium (or low?) Measurement complexity: medium	3
RNA loading	LC-MS/MS	Total mRNA	LC: separation by chromatographic chemical interaction with column MS/MS: fragmentation of molecular ions and detection of mass per charge of fragments	yes	Cannot differentiate between free *vs* encapsulated	Cost: high Measurement complexity: high	1–2
	Fluorescence methods	Total mRNA Loaded *vs* encapsulated mRNA Encapsulation efficiency (%)	Fluorescent dye binding to RNA	yes	Variability introduced by sample preparation	Cost: low Measurement complexity: low	2
	HPLC-UV	Total mRNA Loaded *vs* encapsulated mRNA Encapsulation efficiency (%)	Separation with affinity chromatography, UV detection of RNA bases	yes	Potential interaction with the column	Cost: medium Measurement complexity: medium	3
	Capillary electrophoresis (coupled to LIF)	Total mRNA Loaded *vs* encapsulated mRNA Encapsulation efficiency (%) Size: Molecular weight Integrity/Purity	Separation by size of linearized RNA moving in a gel matrix under electrical field. Detection with fluorescent dye binding to RNA and subsequent laser-induced fluorescence	Yes	mRNA secondary structure can affect the mRNA concentration	Cost: medium Measurement complexity: medium	3
In-vitro Translation efficiency Toxicity Inflammatory response Complement activation	API specific (luminometry)	Efficiency of mRNA uptake and translation, measured as presence of mRNA encoded protein or by its activity (measured here as luminescence).		yes	Toxicity may be interpreted as false negative results	Cost: API-dependent (low). Measurement complexity: API-dependent (low)	3

(*continued on next page*)

Table 5 (*continued*)

Attribute(s)	Measurement technique	Measurands	Physical principle	Applicability	Possible bias	Cost, measurement complexity	Suggested for QC? (1–3)
	Colorimetry and fluorimetry (Absorbance)	Viability and toxicity measured by *e.g.* LDH release and MTT assays		yes		Cost: low Measurement complexity: low	3
	Colorimetric method (Absorbance)	IRF inflammation pathways, using reporter cell lines increasing absorbance upon activation		yes	Toxicity may be interpreted as false negative results	Cost: low Measurement complexity: low	2
	Luminometry	NF-κB inflammatory pathways, using reporter cell lines producing luminescence upon activation		yes	Toxicity may be interpreted as false negative results	Cost: low Measurement complexity: low	2
	Colorimetric methods (Absorbance)	iC3b		yes		Cost: low Measurement complexity: low	1

the particle. Further efforts to develop more robust and reproducible alternatives, *e.g.* the AF4-NTA coupling [35], are necessary to provide robust and reproducible methods for particle concentration measurements.

Measuring efficacy is highly necessary as a regular QC and cannot be substituted by any physico-chemical characterisation assay. As demonstrated in this work, differences in efficacy (*i.e.* level of luciferase activity) could be predicted by the measured total RNA loading and by the DSC profiles, while physical measurements of particle size and aggregation were not so informative in discriminating between LNP2–1 and LNP2–2 batches.

The correlation between physico-chemical properties and concomitant efficacy and safety is one of the most interesting challenges of LNP-RNA therapeutics. None of the physico-chemical tools used in this study can fully explain how the particle structure and dynamic behaviour in physiological conditions influence safety and efficacy. However, the combination of the characterisation results from more methods and the evaluation in a multidimensional parametric space allows to identify the characteristics leading to better efficacy and to better control the effects of synthesis parameters.

3. Conclusions and outlook

The scope of this study was to assess the product quality of LNP-RNA formulations by measuring several physico-chemical properties and linking them to *in-vitro* activity and safety. This was achieved by measuring physical-chemical quality attributes of various LNP-RNA formulations (particle size distribution, particle concentration, mRNA content, lipid content) and analysing the relative performances of different analytical techniques in measuring each quality attribute.

Based on the comprehensive results described in this study, and the experience from nanomedicines we can suggest a good-practice process for routine characterization of LNP-RNA formulations in pre-clinical development. This minimalistic characterization involves measuring particle size distribution and quantification of the total RNA content followed by *in-vitro* activity measurement. Table S6 reports the results of such minimal physicochemical characterization for additional LNP-mRNA formulations.

We would like to stress that the above is really the minimal set of measurements to be used for routine quality control of each of pre-clinical batches and that an accurate, in-depth characterization of any new LNP-RNA formulation would require a more extensive characterization including the quantification of lipids content, morphology of the LNP-RNA particles, and more. This in-depth analysis is critical for getting a comprehensive understanding of the properties and feature of each LNP-RNA formulation, and to understand what happened in the case of problematic synthetic batches. We also want to remark that assessing the quality of production batches for human use requires measuring many more properties than the minimalistic set described above.

Determination of particle size distribution is challenging, and FDA recommends using orthogonal techniques for measuring it. Based on our results a best practice would use a combination of low-resolution techniques for a first assessment (such as DLS or NTA), followed by more complex orthogonal technique such as AF4 coupled with MALS, or AUC. In fact, our data indicate that DLS (and to a lesser extent NTA) can identify some differences between the three batches of LNP-2, while AF4-MALS and AUC can detect multiple population in polydisperse LNP-RNA formulations.

Total RNA content is a key parameter that measures the amount of active pharmaceutical ingredient (API) present in the formulation. Also, in this case we would suggest a combination of a simplified technique based on fluorescence (such as the widely used ribogreen assay) followed by more accurate orthogonal one based on either capillary electrophoresis or HPLC separation with UV or MS detection (Table 5). Our results show that total RNA can be quantified by the newly developed method based on LC-MS/MS with a reproducibility error of around 10% for the different samples (as shown in Table 2).

The tested techniques also provide complementary information that are very useful in the overall characterization of LNP-RNA formulations. NTA gives information on the particle concentration (in addition to particle size distribution); AF4-MALS-DLS give information on the morphology of the particles; AUC provides estimations of the density of the formulations in addition to PSD and DLS (and especially MADLS) can be used as a simple technique to assess aggregation propensities as a function of time, pH, and temperature.

A special case is DSC: it provides a fingerprint of the LNPs structure and composition and can identify differences in structure and composition between batches, making it an effective tool for quality control purposes. In addition, it could also provide complementary information on structural changes in the RNA molecules and the lipids forming LNP particles.

In vitro measurements of activity and toxicity are essential before moving into animal studies (both for ethical considerations and experimental costs). *In-vitro* activity is a key quality attribute that allows to compare the relative potency of different formulations, modifications of the RNA payload and batch to batch assessment. Our results show that it correlates quite well with physico chemical properties (PSD and total RNA loading). Additional *in-vitro* properties, such as endotoxin contamination, cytotoxicity (using MTT and LDH assays) and inflammatory response should also be measured before moving to animal studies.

This work highlights the value of comparative studies involving different laboratories, with interdisciplinary expertise, measuring the

same batch samples. Problematic batches turn out to be extremely useful in linking physico-chemical attributes to *in-vitro* activity and in assessing the capacity of different techniques to identify them. A key message is the importance of combining orthogonal measurements when assessing key physico-chemical properties, such as size, of LNP-RNA systems.

Given the complexity and the potential of RNA therapeutics, international collaboration is essential in the development of measurements and standards for LNP-RNA systems, in line with similar requests coming from both regulators [36,37] and policymakers [38]. This study represents an initial step of larger pre-normative and standardization initiatives at European and international levels, to support ongoing and future projects within the ISO TC 229, CEN TC 352, ASTM E56, and European Pharmacopeia Commission committees.

4. Methods

4.1. Reagents

Ultrapure water (18.2 MΩ cm) for the preparation of the carrier liquids for the AF4 was obtained from a Milli-Q system (Integral 5 system, Merck KGaA, Germany). 1,2-distearoyl-sn-glycero-3-phosphocholine (DSPC) and PEG2000-DMG were purchased from Sigma Aldrich (Avanti Polar lipids), MC3 and SM-102 from Organix (USA), the FLuc CleanCap® FLuc mRNA (5moU) from Tebu-Bio (Roskilde, Denmark). Bovine serum albumin (BSA), monomer ≥97%, foetal bovine serum (FBS), phosphate buffered saline (PBS) tablets were purchased from Sigma Aldrich. Potassium dihydrogen phosphate, disodium hydrogen phosphate dihydrate and sodium hydroxide solution (1 M) were obtained from ChemSolute (Th. Geyer GmbH & Co. KG, Germany), potassium chloride from Carl Roth (Germany) and sodium chloride from Avantor Performance Materials Poland S.A. Sucrose (≥99.9%, Ultrapure DNAse-, RNAse-free) was obtained from VWR. All buffers were filtered through a PES 0.2 um pore size filter membranes before use.

4.2. LNP synthesis

LNPs were synthesized by Lab 1 using the Nanoassembler instrument (Precision Nanosystems) and shared among the partners. Stock solutions of cholesterol, DSPC, and PEG2000-DMG were prepared at 10 mg/mL in EtOH and of MC3 or SM-102 at 20 mg/mL for LNP1 and LNP2, respectively. Three batches using SM-102 (LNP2 samples) and one batch using MC3 (LNP1) were synthesized. Lipids were mixed at a molar ratio of 50:38.5:10:1.5 MC3/SM-102:cholesterol:DSPC:PEG2000-DMG and the EtOH volume was adjusted to obtain a 6.18 mg/mL total lipid concentration. The CleanCap® FLuc mRNA (5moU) was dissolved in RNase-free 25 mM acetate buffer (pH 4.0) at 100 μg/mL concentration. The lipid mixture in EtOH and the mRNA solution in acetate buffer were mixed in a Nanoassembler at a 1:3 volume ratio resulting in a total lipid to mRNA mass ratio of 23.5:1. After formulation, LNPs were dialysed using 10 kDa molecular weight cut-off dialysis cassette (Slide-A-Lyzer™ G2 Dialysis Cassettes, Thermo Scientific™) overnight at 4 °C against PBS 154 mM, pH 7.4 for LNP1 and Tris buffer 10 mM, pH 7.4 plus 10% sucrose for LNP2.

4.3. Lipid composition

Lipid composition measurement of LNPs was performed by high performance liquid chromatography (Agilent 1290 Infinity II, Agilent, Santa Clara, California, USA) with mass spectrometric detection (Agilent 6495 Triple Quadrupole, Agilent, Santa Clara, California, USA). In short, 50 μL of LNP solution was transferred to a 1.5 mL plastic HPLC vial and 450 μL of 20% chloroform in methanol was added before the sample was vortexed for 15 min. From this stock, a 1:10, 1:50, 1:100 and 1:1000 dilution was made to span the concentrations and the very different response factors of the different lipids. Deuterium-labelled lipids were utilized as internal standards for cholesterol, DSPC, MC3 and SM-102, while DSG-PEG2000 was used as internal standard for DMG-PEG2000. Quantification was achieved by utilizing a calibration curve spanning from 0.07 to 100 μg/mL for DGM-PEG2000, cholesterol and DSPC while the concentration range 0.008–12 μg/mL was used for MC3 and SM-102. Chromatographic separation of the different lipids was performed utilizing a Waters C18 BEH Column (2.1 × 50 mm, Waters corp., Milford, Massachusetts, USA) with precolumn. As solvents, water and isopropanol were utilized, both containing 10 mM ammonium formate and 0.1% formic acid. Separation was achieved by a linear gradient from 40 to 100% isopropanol over 10 min. Quantification was done by MassHunter Quantitative Analysis v B.09.00. To ensure the quality of all measurements, two samples of known lipid compositions were included for QC purposes.

4.4. Quantification of total mRNA loading by nucleotide digestion followed by LC-MS/MS

mRNA was extracted from LNPs with Triton-X100 at a final concentration of 1% *v*/v incubated at 37 °C for 15 min. mRNA precipitation was performed by adding, to 150 μL sample of disrupted LNP formulation, i) 15 μL CH_3COONa 3 M pH 5.5; ii) 3 μL of a 20 mg/mL RNA grade glycogen (R0551, Thermo Scientific); iii) 750 μL of −20 °C cold 100% ethanol. After incubation for 1 h at −80 °C and centrifugation, supernatant was removed; the pellet was washed once with 75% cold ethanol, and finally dried under nitrogen. The mRNA was resuspended in nuclease-free water, enzymatically decapped (M0608, New England Biolabs) and finally depolymerized and dephosphorylated using a mixture of *exo*- and *endo*-nucleases in the Nucleoside Digestion Mix (M0649S, New England Bioloabs), all according to manufacturer's instructions. Before nucleoside quantification, ^{13}C labelled stable isotope internal standards were added to the samples. LC-MS/MS quantification was performed on an Agilent 1260 HPLC system, connected to an Agilent 6495 triple quadrupole tandem mass spectrometer operated in positive ion ESI mode. MRM transition and key instrument parameters for the analytes and their internal standards are given in Supplementary Table S4. Final quantification of mRNA was performed based on each of the four nucleosides (G, C, A, 5moU), and subsequently averaged over these. All the measurements were performed in triplicates. Results are reported as average ± (SD).

4.5. DLS, MADLS and Zeta potential measurements

DLS and zeta potential measurements of RNA-LNPs were performed on a Zetasizer Nano ZS system (Malvern Panalytical) following the SOP developed by EUNCL ([15], item EUNCL-PCC-01). MADLS was performed out using a Zetasizer Ultra Red (Malvern Panalytical Ltd., Malvern, UK) as described in Markova et al., 2022 [24].

For size measurements, the LNPs were diluted 50× in sterile filtered PBS pH 7.4 and measured at 20 °C. The average *Z*-average hydrodynamic sizes and PDI values were obtained from a second order cumulants analysis according to ISO 22412 by averaging 10 replicate measurements (DLS) or 3 replicate measurements (MA)DLS [39].

For zeta potential measurements, the particles were diluted 10× in sterile, filtered 10% (*v*/v) PBS, pH 7.4. Five replicates per sample were measured. Zeta potential measurements were performed in a disposable folded capillary zeta cell (DTS1070, Malvern Panalytical), applying the standard operating procedure (SOP) developed by the EUNCL laboratory [15]. pH titrations of the mRNA-LNPs prepared in 10 mM NaCl (10 mL sample volume) were performed with the multipurpose titrator 3 (MPT3) accessory, degasser and Zetasizer Ultra Red at a temperature of 25 °C as described in Markova et al. [24].

4.6. Multi detector AF4 analysis

MD-AF4 measurements were performed with the optimized protocol reported in Mildner et al. [29] following the SOP developed by EUNCL

([15], item EUNCL-PCC-22) and the criteria reported in ISO/TS 21362:2018 [34]. The measurements were replicated by two laboratories equipped with a AF2000 Multiflow FFF (Postnova Analytics, Germany) including the necessary isocratic pump(s), degasser, and autosampler injectors. The AF4 separation was performed on the frit inlet fractionation channels from Postnova Analytics with a tip-to-tip length of 277 mm. The channel temperature was stabilized at 25 °C using a channel thermostat. The autosampler temperature was set to 4 °C. Additionally, the platforms were equipped with 3 online detectors relevant to the present work— multi-angle light scattering detector (PN3621), UV–Vis absorbance detector (PN3211) and differential refractive index detector (PN3150). For the measurement of the hydrodynamic diameter online, Lab 1 was equipped with a Zetasizer Nano ZSP system (Malvern Panalytical) while Lab 2 was equipped with a NanoSight NS300 in the online configuration mode as described in Drexel et al. [35]. The online DLS measurements were carried out at a 173° backscattering angle at a temperature of 25 °C. The online DLS measurement time was kept constant for all measurements with 5 s. The Berry-method with a linear fit was applied to calculate the radius of gyration from the angular dependent scattered light using an angular range from 28° to 148° MALS, considering a minimum of 11 active angles. The AF4 fractionation method was optimized previously [29]. and is displayed in fig. S1. Common conditions used for the fractionation were: (i) injected sample volume: 25 μL of the samples diluted 2.5× (total injected mass: 8–50 μg); (ii) membrane: 10 kDa regenerated cellulose; (iii) mobile phase: isotonic PBS pH 7.4; (iv) spacer height: 350 μm; (v) tip flow (FI channel): 0.2 mL/min; (vi) detector flow: 0.5 mL/min. UV signal was monitored at 230 nm, and was used to calculate the sample recovery as described in ISO/TS 21362:2018 [19]. Three replicates per sample were measured in each laboratory per condition tested.

4.7. Nanoparticle tracking analysis (NTA)

NTA measurements were performed by three laboratories, two of them (Lab 1, Lab 3) equipped with a NanoSight NS300 instrument (Malvern Panalytical) and a third lab (Lab 4) equipped with a NanoSight NS500 instrument according to the EUNCL SOP ([15], item EUNCL-PCC-023). Immediately prior to the measurements LNPs were diluted 10,000× (Lab 1, Lab 3) and 5000× for LNP1 and 20,000× for LNP2s (Lab 4) respectively in PBS. A 405 nm laser was used to visualise particles present in a given field of view. Five recordings of the laser interacting with particles were captured, each for 60 s, using an EM-CCD (NS500) or a SCMOS camera (NS300) for each analysis. The sample was loaded in a dry flow cell and at least 500 μL were flushed in the flow cell prior to analysis. The camera level and focus were manually controlled and set to level 14 or 16, focus 0–60. The detection level was optimized by the operator (typical value of DT═5) and the recordings were subsequently analysed using NTA3.2 (for Lab1, and Lab4) and NTA3.4 (Lab3) software to determine particle numbers per frame and sample concentrations. The reported numerical values are the average of 5 measurements. Measured number-weighted distributions for all samples were averaged over 5 repeated runs or showed separately depending on the purpose of the figure. Before dilution in PBS, the diluents were checked for particles at cameral level 16. As PBS showed no particles, no further filtration was used.

4.8. Size Exclusion Chromatography (SEC-MALS)

SEC-MALS-UV-dRI was performed by one laboratory, using the AF2000 Multiflow FFF (Postnova Analytics) setup used in SEC mode and equipped with a TSKgel-G6000PWxl column of dimensions 8 mm × 300 mm and 13 μm particle size (TOSOH Bioscience, Tokio, Japan) with 1× PBS as mobile phase at 0.5 mL/min flow rate and room temperature column temperature. UV signal was monitored at 230 nm, and was used to calculate the sample recovery adopting the same approach used for the MD-AF4 measurements as described in ISO/TS 21362:2018 [19].

4.9. Differential scanning calorimetry (DSC)

DSC was performed by one laboratory using a MicroCal PEAQ DSC automated (Malvern Panalytical, Northampton, MA, USA) as described in Markova et al. [24]. Briefly, MicroCal PEAQ DSC automated was used for analysis of thermal stability of LNP2–1 and LNP2–2 solutions. For the analysis, 325 μL aliquots of the samples and matching buffer solutions were loaded onto a 96-well plate, covered with a silicon seal, and placed into the PEAQ DSC plate stacker thermostated at 10 °C. The thermal scans were performed in the range from 4 °C to 100 °C or from 4 °C to 130 °C at a scan rate of 60 °C/h. The data were analysed with dedicated PEAQ DSC Analysis software (Malvern Panalytical, Northampton, MA). The resulting normalized and baseline-corrected DSC traces of the LNP2 samples were analysed for temperature of the peak maximum (Tms) and total heat effects.

4.10. Analytical ultracentrifugation (AUC)

AUC measurements were performed by one laboratory. PBS buffer solutions were prepared in water (MilliQ) and deuterated water (D_2O, Sigma-Aldrich, Germany) from PBS tablets (Gibco) to obtain various *v*/v % D_2O solutions (20, 30, 40, 50, 60). Samples were diluted ten times in the various PBS buffers (*i.e.* 40 μL added to 360 μL buffer) measuring also the mass of added aliquots.

Reference solvents were prepared by diluting the buffer used at sample preparation (PBS or Tris-HCl with sucrose) at the same volumetric proportions. Density of the reference buffers was measured at 20 °C by an Anton Paar densimeter DMA 5000, while viscosity was determined using an Anton Paar Lovis 2000 M rolling ball viscometer. Floatation velocity experiments were performed using a Beckman Coulter Proteomelab-XL-I analytical ultracentrifuge equipped with an 8 hole rotor at 10000 rpm rotational speed at 20 °C in double sector sapphire cells. Interference signal and absorption profiles at 220 nm and 260 nm were registered for each sample. Sedimentation coefficient distributions of the lipid nanoparticles at various buffer densities were determined using the ls-g*(s) model of Sedfit [40] using a negative sedimentation coefficient (s) range for the fit. Density of the buffers was plotted against the mode of the resulting s distributions (without correction for viscosity) and density of the particles was estimated by linear extrapolation to 0 sedimentation coefficient [25]. The standard deviation on the density values is calculated by considering the 95% confidence interval is intercept ±2*standard error of the intercept obtained by the Origin 8.0 software. The partial specific volume derived from this value was applied for each sample (together with measured liquid density and viscosity data) to calculate size distributions from interference and absorbance based s distributions. Finally, the results provided by the software were multiplied by −1 (considering that the particles were floating. *i.e.* showed a negative sedimentation speed).

4.11. Cytotoxicity evaluation on Hep G2 cell line

In-vitro cytotoxicity studies were performed by the colorimetric LDH and MTT assays on Hep G2 cells in two labs (Lab 1 and Lab 5) for 24 and 48 h exposure, according to the EUNCL SOP ([15], item EU-NCL-GAT-02). HeP G2 cell line was selected as one of the suggested cell lines indicated in, ASTM and ISO [17,18].

The release of the cytosolic enzyme lactase dehydrogenase (LDH) correlates with membrane disruption/cell death, whereas the cleavage of the chromogenic substrate MTT correlates with the cell metabolic activity and therefore with the number of living cells. Hep G2 cells were plated in 96-well cell culture plates (Corning Inc., Corning, NY, USA) at a density of 5×10^4 cells/well and allowed to adhere for 24 h, then exposed to the LNP-mRNA system for 24 h. Medium control and positive control (Triton 0.1%) were included in each assay. At the end of the exposure time, 50 μL of supernatant was transferred to a new plate for measuring the release of LDH, which was performed with the BioVision

LDH-cytotoxicity colorimetric kit (cat. K311, BioVision, Inc., Milpitas, CA, USA) according to the manufacturer's instructions. Cell viability was evaluated using MTT [3-(4,5-dimethylthiazol-2-yl)-2,5-diphenyl-2H tetrazolium bromide] (Sigma-Aldrich, Inc.) added to the cells in fresh complete culture medium at a final concentration of 250 μg/mL. After 4 h of incubation at 37 °C the supernatant was removed and the precipitated formazan crystals (indicative of mitochondrial metabolic activity, *i.e.*, presence of viable cells) were dissolved in 200 μL DMSO (Sigma-Aldrich, Inc.) followed by 50 μL of glycine buffer (0.1 M glycine with 0.1 M NaCl). The absorbance was quantitated at 490 nm and 570 nm for LDH and MTT assay, respectively, by the EnSpire® Multimode plate reader (Perkin Elmer) using a reference wavelength of 680 nm. Data are expressed as percent of total LDH release and as percent of mitochondrial activity and reported as mean ± SD. All the experiments were performed in triplicates. The data reported in Fig. 5 (Lab 2) and in Fig. S9 (Lab 5) are normalized either for the measured concentration of the total lipid or of the total mRNA amount.

4.12. Morphological observation

Cells were imaged with a Carl Zeiss Axiovision microscope after 24 h, using a 10× objective. Images are shown in Fig. S10.

4.13. Complement activation assay

Measurements were performed according to the EUNCL SOP EUNCL-ITA-10 (available at [15]), adopting a protocol currently under standardization within the ASTM E56 committee LNP-RNAs were prepared in sterile PBS at the concentration of 5×, 10×, 30× diluted from the initial stock concentration and mixed 1:3 *v*/v with normal human Quidel serum (cat. A113; Quidel, Santa Clara, CA, USA). PBS and 0.5 mg/mL Cobra Venom Factor (CVF; cat. A114; Quidel) were included as negative and positive controls, respectively. The quidel serum was selected: i) to reduce individual variability and ii) to limit ethical issues linked to the use of human blood donors. Samples were incubated in a final volume of 150 μL for 1 h at 37 °C under orbital shaking at 300 rpm. Then, 20 μL of EDTA 200 mM pH 8.0 were added to block the reaction. The generation of the complement cascade cleavage products iC3b was tested with commercial Enzyme-linked Immunosorbent Assay (ELISA) kits (cat. A006; Quidel), according to the manufacturer's instructions after appropriate dilution in specimen diluent (1:150). The presence of iC3b was measured with an EnSpire® Multimode plate reader (Perkin Elmer) at 405 nm. A technical replica was run in the ELISA. Results are reported as the average of measurement duplicates ± SD.

4.13.1. Raw-Dual assays

RAW-Dual cells were used in this study, which are commercially available and generated from RAW 264.7 murine macrophages. Thy are part of a kit from RAW-Dual™ cells | IFN & NF-κB reporter macrophages (Invivogen.com) which express many pattern recognition receptors (PRRs) such as the Toll-like receptors (TLRs) TLR2 and TLR4, the cytosolic DNA sensor cGAS, and the cyclic dinucleotide sensor STING. As a result, RAW-Dual cells allow to simultaneously studying the NF-κB pathway, by assessing the activity of SEAP, and the IRF pathway, by monitoring the activity of Lucia luciferase.

Raw Dual cells were plated in 96-well cell culture plates (Nunc, 3598) at a density of 5×10^4 cells per cm^3 and exposed to the indicated concentrations of LNP-mRNA for 24 h. Pam3CSK4 (InvivoGen, cat# tlrl-pms) or 2′3′-cGAMP (InvivoGen, cat# tlrl-nacga23–02) were used as positive controls, whereas media as negative control. The expression of SEAP and Lucia luciferase were assessed with QUANTI-Blue (QB) solution (InvivoGen, cat# rep-qbs2) and QUANTI-Luc solution (InvivoGen, cat# rep-qlc1), respectively. The positive controls and the assay solutions were prepared according to the manufacturer's instructions. Briefly, 24 h after exposure, cell supernatant was transferred to new plates. For the QUANTI-Blue assay, 20 μL cell supernatant was moved to a flat-bottom well plate (Nunc, 3598) together with 180 μL QB solution. Following incubation at 37 °C in a CO_2 incubator for 1–6 h, absorbance was read in a spectrophotometer at 620–655 nm. For the QUANTI-Luc assay, 20 μL cell supernatant was moved to a white well plate (Thermo Scientific™, 136,101) together with 50 μL QUANTI-Luc solution. Following gentle mixing, luminescence was read in a plate reader using 0.1 s reading time.

4.13.2. Endotoxin contamination

Endotoxin contents were evaluated with PyroGeneTM rFC Recombinant Factor C Assay (Lonza, Catalog number: 50–658 U). The standards for the calibration curve were prepared according to the manufacturer's instructions. The standards and controls were plated to a 96-well plate (LAL Reagent Grade Multi-well Plates, Lonza, 25–340) in triplicates, 100 μL/well. The samples were serial diluted 1:100, 1:1000, 1:10000 and 1:100000 in endotoxin-free water, and plated in six replicates. Three of each sample replicates were spiked with endotoxin contents, as well as the positive control. The plate was incubated at 37 °C for at least 10 min, while the working reagent was mixed. Working reagent was added to all wells (100 μL/well) and mixed gently by tapping the plate. The plate was immediately placed in a plate reader (Tecan infinite 200 Pro, Tecan i-control 1.10.4.0) and fluorescence was read at 380/440 nm from the bottom of the plate, using an integration time of 20 μs. The plate was incubated for 1 h at 37 °C, before the fluorescence was read again. Results are reported in Table S5.

4.14. In-vitro luciferase expression

Hep G2 cells were plated in 96-well cell culture plates (Corning Inc., Corning, NY, USA) at a density of 5×10^4 cells/well and allowed to adhere for 24 h, then exposed to the indicated concentrations of LNP-mRNA for an additional 24 h. Separate wells were transfected with FLuc mRNA as positive control, using Lipofectamine™ MessengerMAX™ Transfection Reagent (ThermoFisher, Catalog number: LMRNA001) according to the manufacturer's instructions, using 20 ng FLuc mRNA and 0.15 μL Lipofectamine transfection reagent per well. Expression of firefly luciferase was assessed with the Pierce™ Firefly Luciferase Glow Assay Kit (ThermoFisher, Catalog number: 16176) according to instructions. Briefly, 24 h after transfection, cells were washed once in PBS and lysed in 50 μL 1 × Cell Lysis Buffer. Following incubation at room temperature for 20 min, 20 μL of the lysates were moved to a white 96-well plate (PerkinElmer), and 50 μL 1 × D-Luciferin diluted in Firefly Glow Assay Buffer were added. Cell Lysis Buffer, D-Luciferin, and Firefly Glow Assay Buffer were all supplied with the kit. Following incubation at room temperature for 10 min, luminescence was read in a Tecan Spark plate reader, using an integration time of 1000 ms per well. The data reported are normalized to the measured concentration of total RNA.

Supplementary data to this article can be found online at https://doi.org/10.1016/j.jconrel.2024.01.037.

Funding sources

The study was partially supported by the EU Joint Research Centre through the work programme "Preparedness And Innovation To Tackle Health Challenges" (32401 -PITCH) and within the Portfolio "Better Preparedness and Response To Health Crises" (27- BREATH). G.V., A. P. M. and all SINTEF affiliated authors would like to acknowledge the financial support from the E.C. H2020 project EXPERT under grant ref. 825828

CRediT authorship contribution statement

Jeremie Parot: Writing – review & editing, Writing – original draft, Methodology, Investigation, Formal analysis, Conceptualization. **Dora Mehn:** Writing – review & editing, Methodology, Investigation, Formal

analysis, Conceptualization. **Hanna Jankevics:** Writing – review & editing, Investigation, Formal analysis. **Natalia Markova:** Writing – review & editing, Supervision, Investigation, Formal analysis. **Michele Carboni:** Writing – review & editing, Methodology, Investigation, Formal analysis. **Camilla Olaisen:** Writing – review & editing, Investigation, Formal analysis. **Andrea D. Hoel:** Writing – review & editing, Investigation, Formal analysis. **Margrét S. Sigfúsdóttir:** Writing – review & editing, Investigation, Formal analysis, Data curation. **Florian Meier:** Writing – review & editing, Methodology, Investigation, Formal analysis. **Roland Drexel:** Writing – review & editing, Investigation, Formal analysis, Data curation. **Gabriele Vella:** Writing – review & editing, Investigation, Formal analysis. **Birgitte McDonagh:** Writing – review & editing, Methodology, Investigation, Formal analysis. **Terkel Hansen:** Writing – review & editing, Writing – original draft, Supervision, Methodology, Formal analysis, Conceptualization. **Huong Bui:** Writing – review & editing, Investigation, Formal analysis. **Geir Klinkenberg:** Writing – review & editing, Supervision, Methodology, Formal analysis, Conceptualization. **Torkild Visnes:** Writing – review & editing, Methodology, Investigation, Conceptualization. **Sabrina Gioria:** Writing – review & editing, Writing – original draft, Supervision, Methodology, Investigation, Formal analysis, Conceptualization. **Patricia Urban-Lopez:** Writing – review & editing, Methodology, Investigation, Data curation. **Adriele Prina-Mello:** Writing – review & editing, Writing – original draft, Supervision, Methodology, Formal analysis, Conceptualization. **Sven Even Borgos:** Writing – review & editing, Writing – original draft, Supervision, Methodology, Formal analysis, Conceptualization. **Fanny Caputo:** Writing – review & editing, Writing – original draft, Supervision, Methodology, Investigation, Formal analysis, Conceptualization. **Luigi Calzolai:** Writing – review & editing, Writing – original draft, Supervision, Methodology, Formal analysis, Conceptualization.

Declaration of competing interest

Roland Drexel and Florian Meier are employees of Postnova Analytics GmbH; Hanna Jankevics, Natalia Markova, Michele Carboni are employees of Malvern Panalytical Ltd. The other authors do not have any conflict of interest to declare.

Data availability

Data will be made available on request.

References

[1] K.S. Corbett, D.K. Edwards, S.R. Leist, O.M. Abiona, S. Boyoglu-Barnum, R. A. Gillespie, S. Himansu, A. Schäfer, C.T. Ziwawo, A.T. DiPiazza, K.H. Dinnon, S. M. Elbashir, C.A. Shaw, A. Woods, E.J. Fritch, D.R. Martinez, K.W. Bock, M. Minai, B.M. Nagata, G.B. Hutchinson, K. Wu, C. Henry, K. Bahl, D. Garcia-Dominguez, L. Ma, I. Renzi, W.-P. Kong, S.D. Schmidt, L. Wang, Y. Zhang, E. Phung, L.A. Chang, R.J. Loomis, N.E. Altaras, E. Narayanan, M. Metkar, V. Presnyak, C. Liu, M. K. Louder, W. Shi, K. Leung, E.S. Yang, A. West, K.L. Gully, L.J. Stevens, N. Wang, D. Wrapp, N.A. Doria-Rose, G. Stewart-Jones, H. Bennett, G.S. Alvarado, M. C. Nason, T.J. Ruckwardt, J.S. McLellan, M.R. Denison, J.D. Chappell, I.N. Moore, K.M. Morabito, J.R. Mascola, R.S. Baric, A. Carfi, B.S. Graham, SARS-CoV-2 mRNA vaccine design enabled by prototype pathogen preparedness, Nature. 586 (2020) 567–571, https://doi.org/10.1038/s41586-020-2622-0.

[2] A.B. Vogel, I. Kanevsky, Y. Che, K.A. Swanson, A. Muik, M. Vormehr, L.M. Kranz, K. C. Walzer, S. Hein, A. Güler, J. Loschko, M.S. Maddur, A. Ota-Setlik, K. Tompkins, J. Cole, B.G. Lui, T. Ziegenhals, A. Plaschke, D. Eisel, S.C. Dany, S. Fesser, S. Erbar, F. Bates, D. Schneider, B. Jesionek, B. Sänger, A.-K. Wallisch, Y. Feuchter, H. Junginger, S.A. Krumm, A.P. Heinen, P. Adams-Quack, J. Schlereth, S. Schille, C. Kröner, R. de la Caridad Güimil Garcia, T. Hiller, L. Fischer, R.S. Sellers, S. Choudhary, O. Gonzalez, F. Vascotto, M.R. Gutman, J.A. Fontenot, S. Hall-Ursone, K. Brasky, M.C. Griffor, S. Han, A.A.H. Su, J.A. Lees, N.L. Nedoma, E. H. Mashalidis, P.V. Sahasrabudhe, C.Y. Tan, D. Pavliakova, G. Singh, C. Fontes-Garfias, M. Pride, I.L. Scully, T. Ciolino, J. Obregon, M. Gazi, R. Carrion, K. J. Alfson, W.V. Kalina, D. Kaushal, P.-Y. Shi, T. Klamp, C. Rosenbaum, A.N. Kuhn, Ö. Türeci, P.R. Dormitzer, K.U. Jansen, U. Sahin, BNT162b vaccines protect rhesus macaques from SARS-CoV-2, Nature 592 (2021) 283–289, https://doi.org/10.1038/s41586-021-03275-y.

[3] Z. Kis, R. Shattock, N. Shah, C. Kontoravdi, Emerging technologies for low-cost, rapid vaccine manufacture, Biotechnol. J. 14 (2019) 1800376, https://doi.org/10.1002/biot.201800376.

[4] European Medicines Agency - Committee for Medicinal Products for Human Use, EPAR Onpattro, INN - patisiran (EMA/554262/2018) (n.d.), https://www.ema.europa.eu/en/documents/assessment-report/onpattro-epar-public-assessment-report_pdf, 2018.

[5] EMA, Spikevax (Previously COVID-19 Vaccine Moderna), Eur. Med. Agency, 2021. https://www.ema.europa.eu/en/medicines/human/EPAR/spikevax (accessed January 6, 2023).

[6] EMA, Comirnaty, Eur. Med. Agency, 2020. https://www.ema.europa.eu/en/medicines/human/EPAR/comirnaty (accessed January 6, 2023).

[7] E. Hemmrich, S. McNeil, Active ingredient vs excipient debate for nanomedicines, Nat. Nanotechnol. 18 (2023) 692–695, https://doi.org/10.1038/s41565-023-01371-w.

[8] G. Guerrini, D. Magrì, S. Gioria, D. Medaglini, L. Calzolai, Characterization of nanoparticles-based vaccines for COVID-19, Nat. Nanotechnol. 17 (2022) 570–576, https://doi.org/10.1038/s41565-022-01129-w.

[9] EMA, ICH Q2(R2) Validation of Analytical Procedures - Scientific Guideline, Eur. Med. Agency, 2018, in: https://www.ema.europa.eu/en/ich-q2r2-validation-analytical-procedures-scientific-guideline (accessed January 6, 2023).

[10] U.F. and D. Administration, Drug products, including biological products, that contain nanomaterials: guidance for industry, 2017.

[11] F. Caputo, D. Mehn, J.D. Clogston, M. Rösslein, A. Prina-Mello, S.E. Borgos, S. Gioria, L. Calzolai, Asymmetric-flow field-flow fractionation for measuring particle size, drug loading and (in)stability of nanopharmaceuticals. The joint view of European Union nanomedicine characterization laboratory and National Cancer Institute - nanotechnology characterization laboratory, J. Chromatogr. A 1635 (2021) 461767, https://doi.org/10.1016/j.chroma.2020.461767.

[12] Characterization of Nanoparticles Intended for Drug Delivery, n.d. https://doi.org/10.1007/978-1-4939-7352-1 (accessed January 6, 2023).

[13] J.D. Clogston, The importance of nanoparticle physicochemical characterization for immunology research: what we learned and what we still need to understand, Adv. Drug Deliv. Rev. 176 (2021) 113897, https://doi.org/10.1016/j.addr.2021.113897.

[14] E.O. Blenke, E. Örnskov, C. Schöneich, G.A. Nilsson, D.B. Volkin, E. Mastrobattista, Ö. Almarsson, D.J.A. Crommelin, The storage and in-use stability of mRNA vaccines and therapeutics: not a cold case, J. Pharm. Sci. 112 (2023) 386–403, https://doi.org/10.1016/j.xphs.2022.11.001.

[15] EUNCL, Assay Cascade (n.d.), https://euncl.org/about-us/assay-cascade/ (accessed January 6, 2023).

[16] ASTM E2526–08, Standard Test Method for Evaluation of Cytotoxicity of Nanoparticulate Materials in Porcine Kidney Cells and Human Hepatocarcinoma Cells, ASTM, 2013 (n.d.).

[17] ISO 10993-5:2009 Biological evaluation of medical devices — Part 5: Tests for in vitro cytotoxicity, (n.d.). https://www.iso.org/standard/36406.html (accessed July 26, 2023).

[18] I.O. for Standardization, ISO/TR 10993-22 Biological evaluation of medical devices–Part 22: Guidance on nanomaterials, ISO Geneva, 2017.

[19] ISO/TS 21362:2018(en), Nanotechnologies — Analysis of nano-objects using asymmetrical-flow and centrifugal field-flow fractionation, (n.d.). https://www.iso.org/obp/ui/#iso:std:iso:ts:21362:ed-1:v1:en (accessed January 6, 2023).

[20] Ph. Eur. Commission kicks off elaboration of three general texts on mRNA vaccines and components - European Directorate for the Quality of Medicines & HealthCare - EDQM, Eur. Dir. Qual. Med. Healthc. (n.d.). https://www.edqm.eu/en/-/ph.-eur.-commission-kicks-off-elaboration-of-three-general-texts-on-mrna-vaccines-and-components (accessed July 26, 2023).

[21] E. Oude Blenke, M.J.W. Evers, V. Baumann, J. Winkler, G. Storm, E. Mastrobattista, Critical evaluation of quantification methods for oligonucleotides formulated in lipid nanoparticles, Int. J. Pharm. 548 (2018) 793–802, https://doi.org/10.1016/j.ijpharm.2017.12.035.

[22] K.J. Hassett, J. Higgins, A. Woods, B. Levy, Y. Xia, C.J. Hsiao, E. Acosta, Ö. Almarsson, M.J. Moore, L.A. Brito, Impact of lipid nanoparticle size on mRNA vaccine immunogenicity, J. Control. Release 335 (2021) 237–246, https://doi.org/10.1016/j.jconrel.2021.05.021.

[23] F. Caputo, J. Clogston, L. Calzolai, M. Rösslein, A. Prina-Mello, Measuring particle size distribution of nanoparticle enabled medicinal products, the joint view of EUNCL and NCI-NCL. A step by step approach combining orthogonal measurements with increasing complexity, J. Control. Release 299 (2019) 31–43, https://doi.org/10.1016/j.jconrel.2019.02.030.

[24] N. Markova, S. Cairns, H. Jankevics-Jones, M. Kaszuba, F. Caputo, J. Parot, Biophysical characterization of viral and lipid-based vectors for vaccines and therapeutics with light scattering and calorimetric techniques, Vaccines. 10 (2022) 49, https://doi.org/10.3390/vaccines10010049.

[25] A. Henrickson, J.A. Kulkarni, J. Zaifman, G.E. Gorbet, P.R. Cullis, B. Demeler, Density matching multi-wavelength analytical ultracentrifugation to measure drug loading of lipid nanoparticle formulations, ACS Nano 15 (2021) 5068–5076, https://doi.org/10.1021/acsnano.0c10069.

[26] F. Caputo, R. Vogel, J. Savage, G. Vella, A. Law, G. Della Camera, G. Hannon, B. Peacock, D. Mehn, J. Ponti, O. Geiss, D. Aubert, A. Prina-Mello, L. Calzolai, Measuring particle size distribution and mass concentration of nanoplastics and microplastics: addressing some analytical challenges in the sub-micron size range, J. Colloid Interface Sci. 588 (2021) 401–417, https://doi.org/10.1016/j.jcis.2020.12.039.

[27] J. Parot, F. Caputo, D. Mehn, V.A. Hackley, L. Calzolai, Physical characterization of liposomal drug formulations using multi-detector asymmetrical-flow field flow fractionation, J. Control. Release 320 (2020) 495–510.
[28] Y. Hu, R.M. Crist, J.D. Clogston, The utility of asymmetric flow field-flow fractionation for preclinical characterization of nanomedicines, Anal. Bioanal. Chem. 412 (2020) 425–438, https://doi.org/10.1007/s00216-019-02252-9.
[29] R. Mildner, S. Hak, J. Parot, A. Hyldbakk, S.E. Borgos, D. Some, C. Johann, F. Caputo, Improved multidetector asymmetrical-flow field-flow fractionation method for particle sizing and concentration measurements of lipid-based nanocarriers for RNA delivery, Eur. J. Pharm. Biopharm. 163 (2021) 252–265, https://doi.org/10.1016/j.ejpb.2021.03.004.
[30] ISO/TS 21362: 2018, Nanotechnologies Analysis of Nano-Objects Using Asymmetrical-Flow and Centrifugal Field-Flow Fractionation, ISO Geneva, Switzerland, 2018.
[31] A.J. Barbier, A.Y. Jiang, P. Zhang, R. Wooster, D.G. Anderson, The clinical progress of mRNA vaccines and immunotherapies, Nat. Biotechnol. 40 (2022) 840–854, https://doi.org/10.1038/s41587-022-01294-2.
[32] F. Sebastiani, M. Yanez Arteta, M. Lerche, L. Porcar, C. Lang, R.A. Bragg, C. S. Elmore, V.R. Krishnamurthy, R.A. Russell, T. Darwish, H. Pichler, S. Waldie, M. Moulin, M. Haertlein, V.T. Forsyth, L. Lindfors, M. Cárdenas, Apolipoprotein E binding drives structural and compositional rearrangement of mRNA-containing lipid nanoparticles, ACS Nano 15 (2021) 6709–6722, https://doi.org/10.1021/acsnano.0c10064.
[33] M.L. Brader, S.J. Williams, J.M. Banks, W.H. Hui, Z.H. Zhou, L. Jin, Encapsulation state of messenger RNA inside lipid nanoparticles, Biophys. J. 120 (2021) 2766–2770, https://doi.org/10.1016/j.bpj.2021.03.012.
[34] J. Viger-Gravel, A. Schantz, A.C. Pinon, A.J. Rossini, S. Schantz, L. Emsley, Structure of lipid nanoparticles containing siRNA or mRNA by dynamic nuclear polarization-enhanced NMR spectroscopy, J. Phys. Chem. B 122 (2018) 2073–2081, https://doi.org/10.1021/acs.jpcb.7b10795.
[35] R. Drexel, A. Siupa, P. Carnell-Morris, M. Carboni, J. Sullivan, F. Meier, Fast and purification-free characterization of bio-nanoparticles in biological media by electrical asymmetrical flow field-flow fractionation hyphenated with multi-angle light scattering and nanoparticle tracking analysis detection, Molecules. 25 (2020) 4703, https://doi.org/10.3390/molecules25204703.
[36] E.M. Agency, EMA Regulatory Science to 2025–Strategic Reflection, European Medicines Agency Amsterdam, The Netherlands, 2020.
[37] Ph. Eur. Commission establishes a new working party on mRNA vaccines - European Directorate for the Quality of Medicines & HealthCare - EDQM, Eur. Dir. Qual. Med. Healthc. (n.d.). https://www.edqm.eu/en/-/ph.-eur.-commission-establishes-a-new-working-party-on-mrna-vaccines (accessed January 6, 2023).
[38] An EU Strategy on Standardisation Setting global standards in support of a resilient, green and digital EU single market, An EU Strategy on Standardisation - Setting global standards in support of a resilient, green and digital EU single market, 2022 (accessed January 6, 2023).
[39] I. ISO, 22412, 2017 Particle size analysis—Dynamic light scattering (DLS), Int. Organ. Stand, Geneva Switz, 2017.
[40] P. Schuck, Size-distribution analysis of macromolecules by sedimentation velocity ultracentrifugation and lamm equation modeling, Biophys. J. 78 (2000) 1606–1619, https://doi.org/10.1016/S0006-3495(00)76713-0.